10 Nucleosynthesis

Roland Diehl

10.1 Introduction

Radioactive decay of unstable nuclei is one of the main γ-ray source processes. The radioactive nuclei are a by-product of nuclear reactions in energetic environments; the weak interaction is in most cases responsible for their transformation into daughter isotopes, with a characteristic 'decay time' τ or 'half life' $T_{1/2} = \tau/ln(2)$. The daughter nucleus is generally created in an excited state; its transition to the ground state often includes electromagnetic transitions, hence emission of line γ-rays with characteristic energy values (see Chap. 11). In radioactive decays of the 'β decay' type, positrons (e^+) are produced, which annihilate upon encounter with their antiparticles, the electrons, to produce characteristic annihilation γ-rays.

Gamma-ray lines thus are causally connected to the nuclear processes of element formation, and their observation makes possible the study of physical conditions in nucleosynthesis sites. The measured γ-ray line intensity translates into the abundance of a specific isotope; hence it constrains the parameters of nuclear reaction networks most directly. In comparison, abundance measurements from other astronomical line observations, atomic or molecular transitions observed in the X-ray to radio regime, generally involve additional assumptions or models of line excitation; therefore the inferred abundances depend on the applicability of these often complex line excitation models.

The 'energetic environments' for nucleosynthesis reactions may be stellar interiors, explosive events such as novae and supernovae, but also high-energy collisions of cosmic ray nuclei and the early universe shortly after the Big Bang.

The initial elemental composition in the universe was established by primordial nucleosynthesis shortly after the Big Bang, producing all the hydrogen and deuterium of the universe (the total hydrogen mass fraction is denoted by X with $X_0 \sim 76$ %), some of the present-day ^{3}He, the major part of ^{4}He (total primordial He mass fraction $Y_0 \sim 24$ %), some ^{7}Li, ^{6}Li, and negligible traces of heavier isotopes ($Z_0 \sim 10^{-5}$ %). Nucleosynthesis inside stars is believed to be the origin of the bulk of elements heavier than He, called 'metals' ('Z') by astronomers. Nuclear reactions inside stars also destroy deuterium and lithium isotopes, reducing them significantly below their initial abundances ('astration'). 'Standard abundances' (Fig. 2.1) have

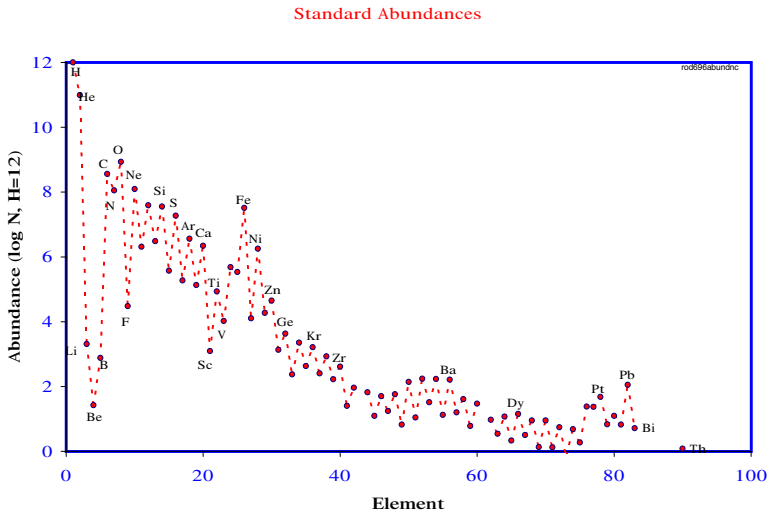

Fig. 10.1. The standard abundances of elements: relative abundances are shown on a logarithmic scale, normalized to hydrogen ($= 10^{12}$). The large dynamic range, but also the regular patterns, are all to be explained by theories of nucleosynthesis. The abundances of specific places, such as the Earth's crust, the interstellar medium in different parts of the universe, or in cosmic rays, deviate in characteristic ways from these 'standard' abundances, which are mostly based on solar-atmosphere and meteoritic measurement.

been assessed, mainly from stellar atmosphere absorption lines and meteoritic analyses (Anders and Grevesse, 1989). This abundance pattern is believed to be representative for large parts of the evolved universe. A metal fraction of ∼2–4% has been contributed by stars during the evolution of the universe. It is the subject of nucleosynthesis and chemical-evolution studies to understand how the primordial elements fit into our understanding of the early universe, and how in detail the enrichment of the full variety of elements in galactic and stellar evolution phases occurred. The observations of radioactivity γ-rays from isotopes with relatively long lifetimes, such that they escape their mostly dense productions sites, allow us to probe these enrichment processes for the recent history of the universe.[1]

Table 2.1 lists the radioactive-decay chains which turn out to be suitable for γ-ray studies of nucleosynthesis. Isotopes with lifetimes $\geq$hours have a

[1] 'Recent' here is determined by the radioactive decay time of the observed isotope, which determines the effective 'exposure' of a gamma-ray line measurement.

chance to escape a rapidly-evolving nucleosynthesis site before decay. On the other hand, when the lifetime reaches millions of years, the sparse amounts of this radioactive trace material from a nucleosynthesis site is insufficient to generate the required γ-ray luminosity to overcome the sensitivity threshold of γ-ray telescopes (see Chap. 3).

Table 10.1. The isotopes relevant for γ-ray line astronomy. ('S' = stars, 'SN' = supernovae, 'N' = novae, 'CR' = cosmic rays, 'Ps' = Positronium)

Isotope	**Lifetime**	**Decay chain**	**Gamma-rays**	**Source**
^{7}Be	77 days	^{7}Be$\rightarrow^{7}$Li*	478	N
^{56}Ni	111 days	^{56}Ni$\rightarrow^{56}$Co$^{*}\rightarrow^{56}$Fe*	847, 1238	SN
^{57}Ni	390 days	^{57}Ni$\rightarrow^{57}$Co$^{*}\rightarrow^{57}$Fe*	122	SN
^{22}Na	3.8 yrs	^{22}Na$\rightarrow^{22}$Ne* + e^{+}	1275, 511	N
^{44}Ti	89 yrs	^{44}Ti$\rightarrow^{44}$Sc$^{*}\rightarrow^{44}$Ca*	1156, 68, 78	SN
^{26}Al	1.04×10^{6}yr	^{26}Al$\rightarrow^{26}$Mg* + e^{+}	1809, 511	S,SN,N
^{60}Fe	2.0×10^{6}yrs	^{60}Fe$\rightarrow^{60}$Co*	1173, 1332	SN
e^{+}	$\sim$10^{5}yrs	e^{+}e$^{-}\rightarrow^{(Ps)}\rightarrow\gamma\gamma(\gamma)$	511	SN,N,CR

The intensity in a specific γ-ray line allows us to derive the present amount of radioactive nuclei of type X (number of nuclei) through

$$n_X = I_\gamma \cdot n_\gamma \cdot 4\pi d^2 \cdot \tau_X, \tag{10.1}$$

with I_γ as measured line flux, n_γ the number of line photons emitted per decay with decay time τ_X of a nucleus of type X, and d the source distance. The originally produced number of radioactive nuclei X then is

$$n_{X0} = n_X \cdot e^{t/\tau_X}. \tag{10.2}$$

For a source located at a distance of d pc, a measurement of γ-rays from species X with n_γ γ-ray line photons of the measured line energy created per decay, and a species X having a molecular weight of m_X and a radioactive lifetime of τ_X years, a line flux of I_γ (photons cm^{-2} s^{-1}) converts into a nucleosynthesis production yield of[2]

$$M_{X0} = 3.12\ x\ 10^{-12} \cdot I_\gamma \cdot \frac{1}{d^2} \cdot \frac{n_\gamma \tau_X}{m_X} \cdot e^{t/\tau_X} (M_\odot). \tag{10.3}$$

[2] The constant 3.12 x 10^{-12} arises from conversion of units, including Avogadro's constant (N$_A$ = 6.022×10^{23} atoms mole^{-1}), the parsec astronomical distance unit (3.085×10^{18} cm), and the mass of the sun (M$_\odot$ = 1.99×10^{33}g). As an example, a 1.156 MeV ^{44}Ti source at the Galactic Center with I_γ = 10^{-5} photons cm^{-2} s^{-1} would correspond to a present ^{44}Ti amount of 9×10^{-6} M$_\odot$ at such a source, consistent with a typical expected Supernova Type II yield of 8.4×10^{-5} M$_\odot$ if the supernova had occurred $\simeq$200 yr ago. Present-day instruments have sensitivities ranging down to a few 10^{-6} photons cm^{-2} s^{-1}. This corresponds to a capability of detecting typically an individual supernova in ^{56}Ni out to 10 Mpc, the near side of the Virgo cluster of galaxies, or 6×10^{-3} M$_\odot$ of ^{26}Al (corresponding to $\sim$ 150 supernovae) at the distance of the Galactic Center.

In this chapter, I describe the individual sites of nucleosynthesis, and I discuss how γ-ray measurements relate to the physics in specific sources and, more indirectly from accumulated radioactivity in extended regions, to the evolution of stellar ensembles. For more in-depth study, I refer the reader to textbooks and recent review articles on nuclear astrophysics (Rohlfs and Rodney, 1988; Arnould and Takahashi, 1999), on nucleosynthesis in general (Clayton, 1968; Arnett, 1996; Pagel, 1997; Wallerstein et al., 1997), and on γ-ray line astrophysics with radioactivities (Diehl and Timmes, 1998). The history of the field of nucleosynthesis is reflected in its foundation paper 'B^2FH' (Burbidge et al., 1957), complemented by other pioneering work (Suess and Urey, 1956; Cameron, 1957; Clayton et al., 1969; Ramaty and Lingenfelter, 1977; Arnett et al., 1977) and reviews (Trimble, 1975, 1991).

10.2 Nucleosynthesis Processes

The energy regime of nuclear reactions may be estimated from the requirement of close encounters of nuclei to within the short range[3] of nuclear forces: Coulomb repulsion between protons places the reaction threshold in the regime of MeV energies. The binding energy of nucleons in the atomic nucleus is of the order 8 MeV nucleon^{-1}, typical nuclear energy-level intervals are in the 100 keV to 1 MeV range. Therefore typical line radiation energies of nucleosynthesis sites are of the order of MeV, about 3–5 orders of magnitude above the regime of atomic transitions. Atomic transitions are the basis of spectroscopy of stellar-envelope and interstellar gas, which allows (mostly elemental, as opposed to isotopic) abundances at those sites to be derived.

Nuclear reactions rearrange the configurations of nucleons inside an atomic nucleus via two physical processes:

- Nuclei collide and approach within the range of strong interactions, and
- Weak-force transitions convert neutrons and protons into each other (β decay).

The weak transitions are (almost) independent of density and temperature, while for collision-induced reactions, collision energy and frequency determine the rate of nuclear reactions. The phase space of daughter states in both cases determines the reaction rate.

In laboratory nuclear reactions, projectile energies are chosen conventionally such that the Coulomb barrier is clearly overcome. In astrophysical environments, on the other hand, the interacting particle population has a broad distribution in energies. In this case, the total reaction rate is a convolution of the reaction cross section (as a function of projectile energy) with the energy distribution of the projectiles. This convolution results in the 'Gamow peak' of the reaction rate versus energy (Gamow, 1928). The reaction cross

[3] The range of nuclear forces is $\simeq$fm $= 10^{-13}$ cm.

section for astrophysical purposes must be known precisely at and around this relevant energy. Typically the Gamow peak energy (in keV) is[4]

$$E_0 = (15.65 \cdot Z_1 \cdot Z_2 \cdot \mu kT)^{\frac{2}{3}}, \tag{10.4}$$

with $\mu = \sqrt{\frac{m_1 \cdot m_2}{(m_1+m_2)}}$ as reduced mass.

'Nucleosynthesis' is the net effect of a complex interplay of many nuclear reactions, whereby material of some initial composition evolves to a different one. The boundary conditions (collision frequency and energy) for the nuclear reactions usually vary during the process. The type of environment has been used to define characteristic 'processes' (Burbidge et al., 1957) which are typical for specific source types, and allow approximations to solve the nucleosynthesis reaction network (see Table 2.2). In the general case, a large set of coupled nonlinear differential equations must be solved in the general case (Arnett, 1996): For species i, the specific abundance is described as a balance between production and destruction,

$$\frac{dY_i}{dt} = Y_k Y_l \rho N_A < \sigma v >_{kl,i} - Y_i Y_l \rho N_A < \sigma v >_{il,j} + Y_j \lambda_{j,i} - Y_i \lambda_{i,l} + ..., \tag{10.5}$$

with terms for all reaction channels that either lead to production or destruction of species i. Here Y_i denotes the relative abundance of species i at their center-of-mass velocities v, N_A the Avogadro number, ρ the mass density, $\sigma_{i,j}$ the reaction cross section between species i and j, and $\lambda_{i,j}$ the decay constant from species i into j. Reaction cross sections $\sigma_{j,i}$ are often steep functions of temperature. The general and time-dependent solution of this network of equations can be very complex. In many cases, however, identification of the most relevant reactions and isotopes reduce the network to a manageable size, thus defining local 'cycles' of reactions, which are only weakly or in a simple way coupled to the rest of the nuclear network (see Table 2.2). [5] Alternatively, thermodynamic treatment of steady-state situations and equilibria provides useful simplifications. Composition changes as part of the process, energy is transferred between its different forms of kinetic and internal energy, and therefore the thermodynamic equations include the chemical potentials:

$$dU = TdS + pdV - \sum \mu_i dY_i. \tag{10.6}$$

The idealized complete equilibrium between all species and fields is called thermodynamic equilibrium. Here matter would adopt its most stable form, Fe group isotopes as most tightly bound nuclei; the isotopic composition

[4] As an example, for the ^{3}He$(\alpha,\gamma)^7$Be reaction at 30 million K the Gamow peak energy is 36 keV.

[5] Examples are the CNO cycle in core hydrogen burning, or the Na–Mg–Al cycle (Fig 2.2).

then depends on the relative numbers of protons and neutrons available at a particular temperature.[6]

Table 10.2. The nuclear-reaction process categories relevant for nucleosynthesis in different astrophysical environments. (SN: supernovae; N: novae; CR: cosmic rays; NSE: nuclear statistical equilibrium; Ps: Positronium formation).

Process	**Description**	**Site**
NSE	All except weak interactions in thermal equilibrium	SNIa, (SNII)
Quasiequilibria	Equilibrium valid only in localized regimes of nuclear chart	Si-burning, hot H burning, etc.
Freeze-out	Equilibrium breaks down as region expands, only a few reactions remain	BBN, SNII/Ib hot bubble
Nonequilibrium	Reaction rate networks to be solved explicitly (no thermodynamic treatment)	Stellar nucleosynthesis
r/s process	Neutron captures and β decays only	SNII/Ib, pulsating stars
p process	Neutron extraction or p capture (also 'γ process')	Novae, SNII
ν process	ν triggered additional spallation	SNII/Ib hot bubble, BBN

Neutrinos are produced in weak decays (e.g., $n \rightarrow p + e + \overline{\nu_e}$), and carry away energy from the reaction site. Therefore complete thermodynamic equilibrium is usually not attained. Rather a 'quasiequilibrium' called 'nuclear statistical equilibrium' (NSE) may be achieved, with all exept weak interactions being in equilibrium. In this NSE state, all strong nuclear reactions [$A(p,x)B$, $A(n,x)B$, $A(\alpha,x)B$, etc., but also $A(\gamma,x)B$] are balanced by their inverse reactions, such that the overall composition is dynamically stable. Because of the different temperature dependencies of the various reaction cross sections, the resulting composition is a function of temperature.[7] NSE burning is probably realized in the most dense and violent nucleosynthesis sites, in thermonuclear supernovae, probably also in inner parts of core collapse

[6] The neutron excess is a characteristic parameter for nucleosynthesis product composition. It may also be measured through the relative abundance of electrons Y_e, as $p + e$ and n are in weak-interaction equilibrium, assuming charge neutrality. For equal numbers of neutrons and protons, $Y_e = 0.5$.

[7] It is advantageous to characterize nucleosynthesis environments through the normalized 'entropy per baryon' rather than by 'temperature' (Meyer, 1993). Then the relative importance of photodisintegration reactions better describe the characteristics of these usually radiation-dominated environments.

supernovae. Radioactive ^{56}Ni is produced in large amounts, when nuclear burning settles to most tightly bound species. Other explosive regimes evolve faster than these equilibration time scales, so that incomplete burning leaves a characteristic abundance pattern.

'Quasiequilibria' may serve as useful approximation to NSE: when changes of abundances Y_i are small compared to the actual rates of production or destruction within a local group of nuclei, equilibrium treatment within this group is allowed. Although NSE is not obtained globally, this significantly reduces the number of reactions that have to be followed explicitly in a reaction network (Arnett, 1996; Hix and Thielemann, 1999). Such a description applies in the r, s, and α processes (Meyer, 1994).

Freeze-out from equilibrium is another useful approximation to characterize the composition from a nucleosynthesis site. Here, an initial equilibrium (or quasiequilibrium) situation experiences rapid dilution, so that nuclear reactions cannot keep up due to the decreasing collision frequency. This results in characteristic modifications of initial abundance patterns, which nevertheless derive from the equilibrium situation in a straightforward manner. Examples are primordial nucleosynthesis in the early universe, but also the 'α-rich freeze-out' from a supernova: at high entropy per baryon, photodisintegration reactions result in an abundance pattern where α nuclei are the most abundant species. The dilution of such an environment due to thermal expansion results in a relative lack of seed nuclei other than α particles, specifically those with odd numbers of nucleons; the most frequent collisions of α particles preferentially build up nuclei composed of α multiples, producing, for example, copious amounts of radioactive ^{44}Ti.

When 'cycles' of nuclear reactions dominate, isotopic abundances are critically determined from the individual nuclear reaction cross sections. Direct, or even indirect, experimental measurements are often difficult, in particular for charged-particle reactions, due to Coulomb repulsion and the dominating tunnel effect (Rohlfs and Rodney, 1988). A prominent example is the $^{12}\mathrm{C}(\alpha,\gamma)^{16}\mathrm{O}$ reaction, a key reaction to generate the seeds for all heavier elements, which controls red giant evolution as well as the chemistry and dust formation in stellar envelopes, which critically depend on the $^{12}\mathrm{C}/^{16}\mathrm{O}$ ratio. This reaction cross section results from details of two subthreshold resonances, and is still a main topic of research; its current value has been inferred from chemical evolution studies, more than from nuclear reaction experiments (Wallerstein et al., 1997). Similarly, measurements of abundances for other intermediate-mass isotopes can help to calibrate nuclear reaction cycles, such as γ-ray line observations of ^{7}Be, ^{22}Na, and ^{26}Al (here in particular the Mg–Al cycle illustrated in Fig 2.2). For some of these isotopes, production in hot hydrogen burning, hence proton-rich environments, through the rp process can be significant (Schatz et al., 1997).

Neutron capture reactions are of special importance in cosmic nucleosynthesis, owing to the absence of Coulomb repulsion. Essentially all elements

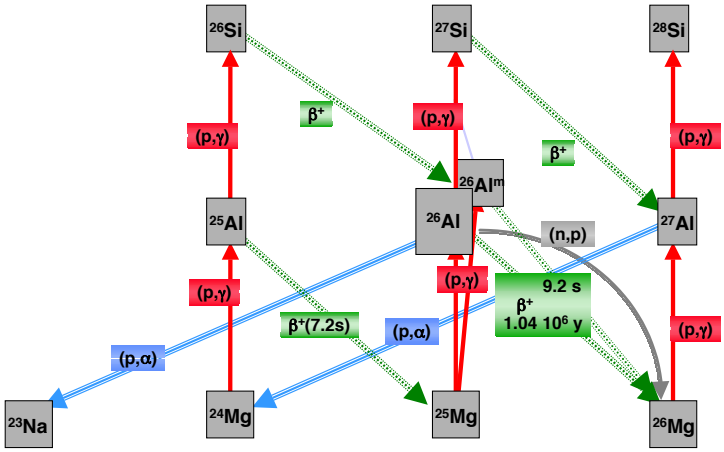

Fig. 10.2. The production of intermediate-mass nuclei occurs in networks of nuclear reactions, involving strong [e.g. (p,γ)] and weak reactions; (p,α) reactions feed back to lighter nuclei and close the cycles, if the (p,γ) break-out reactions are comparatively slow

heavier than iron are produced through successive neutron capture, hence from the seeds of Fe-group elements. In the case of the 'r process', neutron capture reactions are much more rapid than competing β decays. Isotopes are produced far out on the neutron-rich side of the valley of stability near the neutron drip line[8] through an intense (10^{20} neutrons cm^{-3}, $\tau \leq$ seconds) neutron flooding. They relax into the characteristic final r process abundance pattern through β decays (see Fig 2.3). In the other extreme, 'slow' neutron capture drives the 's process' into its characteristic abundance pattern (Käppeler et al., 1989). Here the neutron collision frequencies are much lower (10^8 cm^{-3}), so that between neutron captures all isotopes have time to β decay to their stable daughter products. Therefore the s process populates isotopes along the valley of stability, on the neutron-rich side. The source process is unique for isotopes which are either 'shielded' towards the neutron-rich side by a stable isotope ('s only'), or separated by one or more unstable isotopes from the valley of stability ('r only').

[8] Here the neutron separation energy S_n reaches small values, often reflecting a configuration where all bound neutron states in a nucleus for a given proton number are filled.

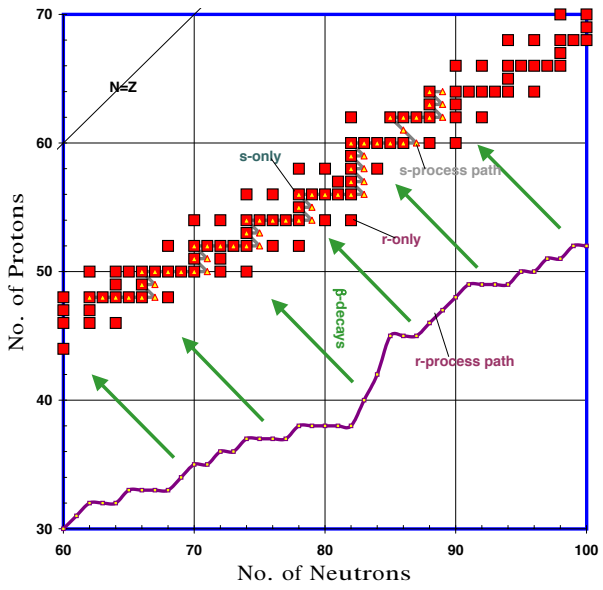

Fig. 10.3. Chart of nuclei, indicating the valley of stable nuclei, and the path of r- and s process nucleosynthesis processes.

For production of isotopes on the proton-rich side of the valley of stability, a 'p process' is invoked. This process is also termed a 'γ process', because (γ, n) reactions yield the same reaction path; it is yet unclear, which reactions produce the 'p isotopes'.

Unfortunately γ-ray-emitting radioactive r, s, or p isotopes are too rare to allow study of the r, s, or p processes through γ-ray line astronomy.

In the inner regions of core collapse supernovae, nuclear reaction sites are exposed to the most luminous neutrino source in the universe, the proto-neutron star. Interactions of neutrinos with nuclei result in spallation, thus releasing additional lighter nuclei, protons and α particles (Qian and Woosley, 1996) and smoothing the abundance distribution. The enhancement of seed nuclei for nuclear reactions (ν process) may increase the production of specific intermediate-mass isotopes such as ^{26}Al by up to 50% (Woosley et al., 1990).

In models of isotopic yields from astrophysical sites, two approaches are common:

- The network is restricted to the nuclear reactions with significant contributions to the total energy budget. This approach is common in stellar-evolution models with a consistent treatment of hydrodynamic and nuclear physics.
- The nuclear processing within a complex network of isotopes is decoupled from the hydrodynamic evolution and applied as post-processing. This approach is common in fast-evolving sites such as novae and supernovae, where the hydrodynamic treatment time scale is thus adapted to the problem, while the detailed composition is evaluated in a secondary step.

Therefore the relation of the measurement of a radioisotope γ-ray line to one of the above physical processes is often indirect.

10.3 Sites of Nucleosynthesis

10.3.1 Hydrostatic Nuclear Burning

In dense astrophysical nucleosynthesis sites, temperatures range over 3–4 orders of magnitude from 10^6 to $5{\times}10^9$ K, densities span even 12 orders of magnitude from 100 nuclei cm^{-3} (hydrogen burning) to 10^{14} cm^{-3} (Si burning in massive stars). The time scales for the different stages of stellar burning are quite different, not only because of the steep temperature dependence of most cross sections, but more so because of the different cooling mechanisms: In the hydrogen- and helium-burning stages, the bulk of the nuclear energy is generated in the form of γ-rays and thus is converted into local heating. This, in turn, results in thermal expansion of the burning site, such that the energy generation rate is reduced. Eventually, radiation transport and thermal expansion will have established hydrostatic equilibrium for the burning stage. This may last billions of years for stars as massive as the sun, while for example stars 25 times as massive would experience stable hydrogen burning only for a million years. From carbon burning onward, a large part of the nuclear-burning energy emerges in the form of neutrinos and hence escapes from the burning region. Therefore these burning stages are much shorter, exhausting their fuel locally at an almost maximum rate. For example, carbon burning for a 25 $M_\odot$ star lasts only 600 yr, and silicon burning just a day.

Even the seemingly stable hydrostatic burning inside stars will evolve significantly after the main-sequence phase of core hydrogen burning. A steady-state description is rarely adequate to model the nucleosynthesis, even less in intermittent nuclear burning in shell-burning stages of massive stars: nuclear-burning time scales become shorter than the hydrostatic-adjustment time scales, and pulsing instabilities are a common characteristic of these stars in their 'giant' stages (Iben and Renzini, 1983).

Stars ascend to the Asymptotic Giant Branch AGB after core ^{4}He burning has been exhausted (Lattanzio and Boothroyd, 1997). The stellar envelope is

enriched by 'dredge-ups' with burning products. In AGB stars, both hydrogen and helium eventually burn concurrently in shells. For low-mass ($\leq$4 $M_\odot$) AGB stars, a flash of helium burning in the inner part will cause expansion of the outer part, and thus extinguish the shell hydrogen burning further out; only after a settling time, will re-started hydrogen shell burning have produced new fuel for this inner-shell helium burning to resume. Thermal-pulsing cycles are the result of this basically unstable situation. Convective energy and material transport ('third dredge-up') characterizes this phase, and the physical environment for nuclear reactions will vary significantly both in time and space. For more massive ABG stars, the bottom of the convective envelope may reach down to the hydrogen-burning shell, so that fresh fuel is supplied to hydrogen burning, turning carbon-rich envelopes resulting from earlier burning stages into oxygen-rich envelopes and producing ^{7}Li and other intermediate-mass isotopes in this 'hot-bottom burning'. Typical envelope turnaround times are $\sim$ 0.5 yr. The outer envelope of AGB stars is weakly bound; strong stellar winds expel substantial parts of the stellar envelope into interstellar space. Therefore the interstellar medium element abundances will be sensitive to how efficiently products from nuclear reactions deeper inside the star can be mixed into the envelope, where the wind is formed. Additionally, the cool outer envelopes favor formation of dust; therefore the laboratory study of presolar dust grains embedded in meteoritic material has been a rich field to analyze and constrain AGB nucleosynthesis (Bernatowicz and Walker, 1997). Due to their relatively long stellar lifetime, in AGB stars even inefficient production processes can become important for the cosmic abundance budget. There is sufficient time for reactions operating in the far tails of the Gamow peak to produce intermediate-mass elements such as Ne, Mg and Al, or for slow neutron capture on prestellar heavy-element seeds to produce rare-earth elements in the s process. The detection of atomic lines from technetium in the atmosphere of an AGB star indeed provided the first unambiguous proof of nucleosynthesis[9] in stellar interiors (Merill, 1952).

The γ-ray radioisotope ^{26}Al may be produced in hydrogen shell burning at temperatures $> 5\times10^7$K. Additionally, in the hot-bottom burning scenario the Mg(p,γ) reaction can produce ^{26}Al very efficiently (even from the more abundant ^{24}Mg isotope), mixing freshly produced ^{26}Al quickly into the wind. Therefore, AGB stars of intermediate mass are candidate ^{26}Al sources. This is true even without hot-bottom burning, due to the third dredge-up and thermal pulses; yet here some ^{26}Al also is expected to be mixed downward closer to the He burning shell, where n-capture reactions quickly destroy it. The large uncertainties of convective processes and intermittent shell burning translate into significant uncertainty in the interstellar nucleosynthesis yields from AGB stars (Forestini and Charbonnel, 1997).

In more massive stars, stellar evolution is initially similar to that described above, with convective-core hydrogen burning. The more massive cores result

[9] Tc has only unstable isotopes, with radioactive decay times $\leq 10^6$ yr.

in higher temperatures, however, so that for stars of $\geq 15 M_\odot$ proton capture reactions can produce fresh isotopes such as ^{26}Al from suitable seed nuclei. Thus, as a by-product of hydrogen burning, ^{26}Al is enriched in the H-burning core and predominantly left behind in the nonconvective outer core as convection recedes during progressive H-burning. The enormous radiation pressure in these stars during the shell burning phase drives a strong wind of 10^{-5}–10^{-4} $M_\odot$ yr^{-1}, quickly removing the inert outer envelope and uncovering the hydrogen-burning layer on time scales of order 10^6 yr. Therefore, for such massive stars, this 'Wolf Rayet' (WR) phase helps to extract ^{26}Al from the earlier H burning phase into the interstellar medium, before it can decay or be destroyed in He-burning, as is the case for stars with $M \leq 20$–40 $M_\odot$, the lower limit for a star to become WR (Meynet et al., 1997). There are interesting deviations from this first-order model for substantial ^{26}Al production by WR stars: stellar rotation may enhance the mixing processes, thus enhancing the supply of seed nuclei for proton capture nucleosynthesis. The high fraction of binary systems (more than 50% of massive stars are members of binary systems) may modify nucleosynthesis of the system: the companion's gravitational pull produces tidal effects, which affect convective mixing of envelope material and hence late evolution; the mass transfer to the secondary enriches its envelope with seed material for more efficient shell burning, with the products then ejected in its supernova.

10.3.2 Explosive Nucleosynthesis

In explosive events such as novae (Gehrz et al., 1998) and supernovae (Burrows, 2000) large-scale hydrodynamical adjustment of the burning site due to the local release of nuclear energy cannot occur, in contrast to the hydrostatic nuclear burning described above. Much higher burning temperatures develop in these sites and result in substantial nuclear processing of material, in spite of the short duration of explosive nuclear burning. Thus, explosive events are prime sites of nucleosynthesis. Additionally, supernova explosions release large amounts of processed material instantaneously, while hydrostatic-burning products have to be mixed into stellar winds to be released into the interstellar medium during the lifetime of a star. Therefore much of the fresh material produced in explosive events ends up as observable chemical enrichment, while much of hydrostatically produced fresh elements are buried in white dwarfs.[10]

Core-Collapse Supernovae

The final stage of stellar evolution will, for stars more massive than about 8–10 $M_\odot$, result in a core of nuclei in their most stable configuration (iron-group elements), thus leaving no nuclear source of energy to halt gravitational

[10] This is not true for the inner regions of a core-collapse supernova.

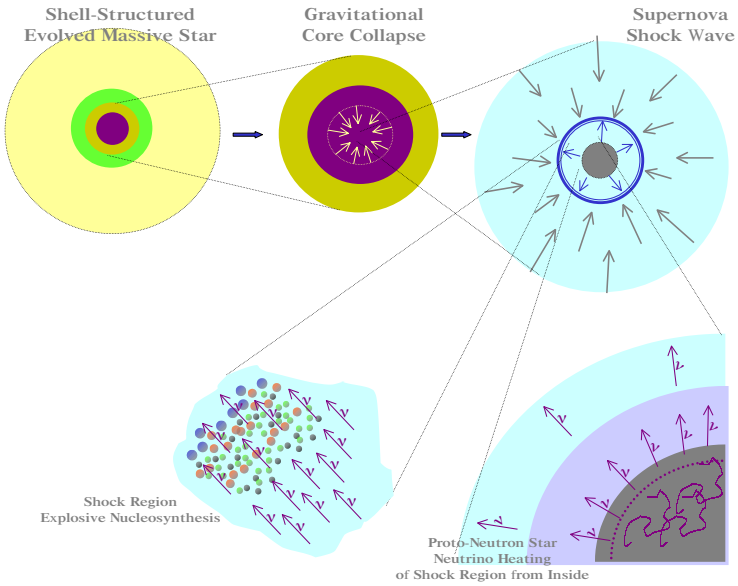

Fig. 10.4. Core-collapse supernovae result from the terminal gravitational collapse of massive star cores. The collapsing matter rebounds when reaching nuclear-matter density; intense neutrino heating from the forming neutron star helps the shock to expand against infalling matter and eject the mantle and envelope. Explosive nucleosynthesis occurs in the shock region

collapse (see Fig 2.4 and (Burrows, 2000)). At this stage such a star, or more precisely its iron core, will undergo gravitational collapse, compressing the nuclei until a new physical limit is reached, where the entire core is just one giant atomic nucleus, i.e. nuclear matter. At this moment, the gravitational collapse is stopped abruptly, resulting in a 'core bounce' shock wave travelling outward. Simultaneously, the protons in the core yield to the high electron pressure and undergo inverse β decay to become neutrons, which can be even more densely packed, reacting to gravitational pressure and decreasing electron thermal pressure. This 'neutronization' results in copious emission of neutrinos, radiating most of the gravitational energy ($\sim 10^{53}$ erg) into the infalling material. At these densities, neutrinos have a significant probability for interacting with nuclei of the surrounding matter within this inner core of $\sim$300 km radius and thus support the struggle of the core-bounce shock wave against the matter falling in from the mantle, eventually reversing the gravitational collapse into an explosion. During this event, nucleosynthesis will occur in two very different environments: close to the proto-neutron star, infalling material is flooded with neutrons and neutrinos, spallation and neutron captures occur at very high rates; further out, an intense shock wave heats up the shells of material (which may have been burning hydrostatically

already; see Fig 2.4), modifying the nuclear reaction environment substantially out through the oxygen shell for a transition period ('explosive nucleosynthesis'). The shock wave energy is eventually sufficient to eject all except the very inner parts close to the forming neutron star, thus enriching the surrounding medium with products of explosive burning and of prior hydrostatic nucleosynthesis.

The genesis of the central compact remnant in core-collapse supernovae includes several interesting physical problems, some of which may be constrained by radioactivity observations. Formation of a neutron star appears likely for main-sequence masses below $\sim$20 $M_\odot$, while a black hole probably forms for main-sequence masses above this regime. The energy of the explosion, the placement of the mass cut[11], and how much mass falls back onto the remnant shortly after the explosion all modify this neutron-star–black-hole bifurcation point. Each of these processes also affects the mass of nucleosynthetic products ejected from the inner regions of the supernova. Note that these supernova parameters are not yet understood and are empirically adjusted in different ways in current models of core-collapse supernova nucleosynthesis (Woosley and Weaver, 1995; Thielemann et al., 1996).

The chief explosive-nucleosynthesis products are nuclei of the iron group, from the inner region where NSE conditions are obtained, and intermediate-mass elements such as oxygen and neon, from burning in the supernova shock wave. Enrichment of α elements is likely, from freeze-out due to the rapid expansion of the main inner burning region. Typically, 0.1 $M_\odot$ of radioactive ^{56}Ni is produced, its rapid decay ($\tau \sim$ days) powers the bright optical display of the supernova. The mass profile of these inner nucleosynthesis products is shown in Fig 2.5.

In supernovae from massive stars, stable ^{44}Ca is produced chiefly, almost exclusively, as radioactive ^{44}Ti in the α-rich freeze-out from the inner part of the supernova. No other ^{44}Ca production process is compatible with the large observed ^{48}Ca/^{46}Ca ratio. Production in core-collapse events after wind loss of the envelope (the 'Type Ib' events)[12] should be more uniform because stellar-evolution models converge to a common presupernova mass in the narrow range $2.3--3.6$ $M_\odot$. All of the models, whose ejecta all have $\sim 10^{51}$ erg of kinetic energy (at infinity), predict ^{44}Ti yields[13] between $1 and 15\ x\ 10^{-5}$ $M_\odot$. Production of more than 10^{-4} $M_\odot$ of radioactive ^{44}Ti is difficult to achieve in such spherically symmetric models adjusted to observables, but ejection of much less seems easily possible. The interstellar ^{44}Ti yield is especially

[11] The mass cut is the separation line between matter that will end up onto the compact remnant by collapse or post-supernova accretion and matter that will be ejected into interstellar space. For neutron-star remnants, it lies in the regime 1.3–1.9 $M_\odot$.

[12] If the envelope of a core-collapse supernova still contains hydrogen, a 'Type II' event results, while absence of a hydrogen envelope identifies 'Type Ib/c' events

[13] Typical values are $\sim 3{\times}10^{-5}$ $M_\odot$ for the Type II models, or twice that value for the Type Ib models.

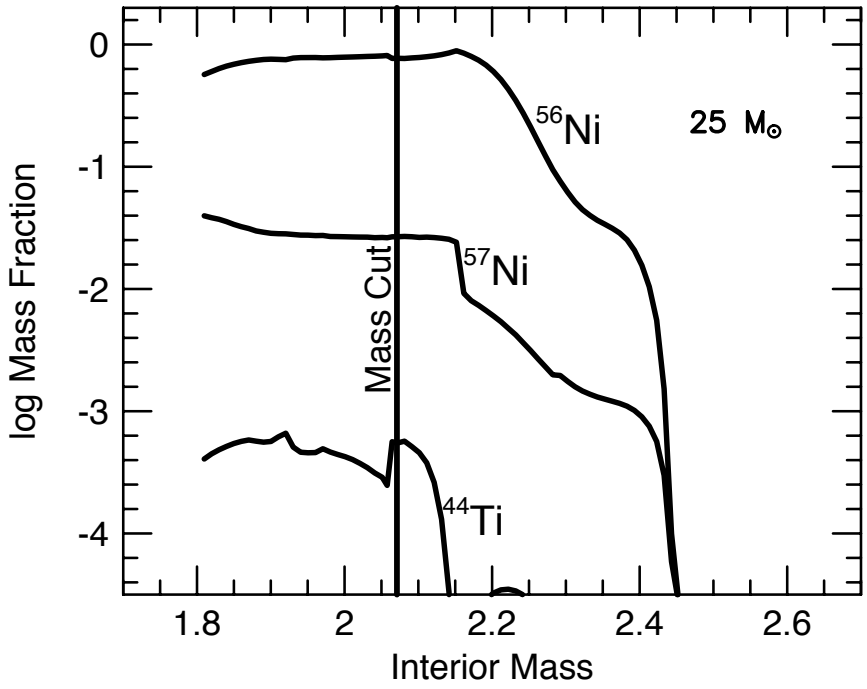

Fig. 10.5. Mass profiles of ^{44}Ti and ^{56}Ni for a 25 $M_\odot$ core-collapse supernova model. The *vertical line* shows the mass cut, separating ejecta from material that ends up on the compact remnant star. Reproduced with permission from Timmes et al., 1996.

sensitive to how much mass falls back onto the remnant. Supernova remnant observations suggest a nearly constant kinetic energy of the ejecta, which implies that the explosion energy in more massive events must be steadily increased in order to overcome the increased binding energy of the mantle. However, even in present 35 and 40 $M_\odot$ models nearly all the produced ^{44}Ti falls back onto the compact remnant. Unless the explosion mechanism, for unknown reasons, provides a much larger characteristic energy in more massive stars, it appears likely that stars larger than about 30 $M_\odot$ will have dramatically reduced ^{44}Ti yields and leave massive remnants ($m \geq 10$ $M_\odot$), which become black holes. Rotation may modify this picture significantly by breaking the spherical symmetry of the explosion. Regions of material with larger entropy could develop behind an asymmetric shock front, and cause a higher ^{44}Ti production, perhaps by as much as an order of magnitude. Plausibly, jets enriched in ^{44}Ti may be induced (e.g. in the polar regions of a rotating supernova), and still remain in agreement with above energy arguments. Birth velocities as high as 1000 km s^{-1} are observed for radio pulsars, and often taken as evidence for some small asymmetry in the explosion of core-

collapse supernova ('kicks'), although magnetic field or ν wind asymmetry provide alternative explanations. Rotation and magnetic fields are a common characteristic of massive stars, and each could induce spatial asymmetries of nuclear-burning conditions. Consistent modelling of such asymmetry has not yet been achieved. Note that in particular nickel isotope ratios can be measured and provide a tight constraint on the entropy/neutron ratio in the inner nucleosynthesis region.

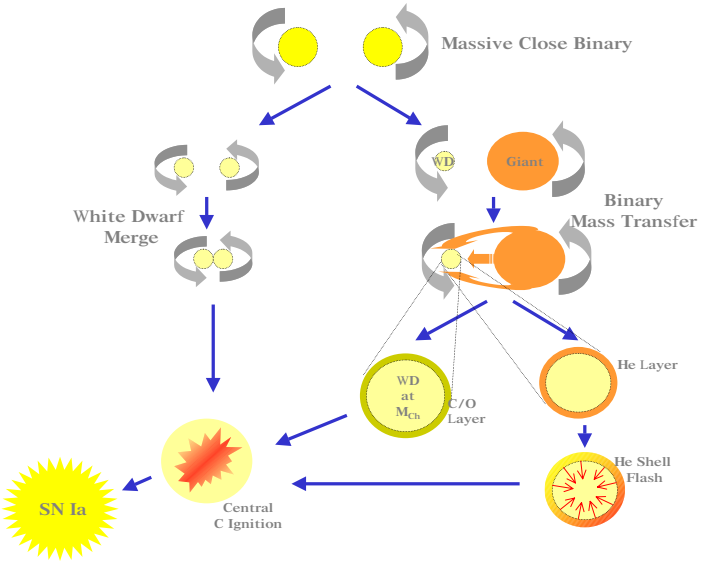

Fig. 10.6. Thermonuclear supernovae result from the explosion of white dwarfs after accretion of matter from a companion induce them to ignite. Central carbon burning in degenerate matter leads to the supernova. Ignition can occur through accretion beyond the Chandrasekhar stability limit or through a shock wave from flash burning of an accreted helium layer. Merging of white dwarfs may be an alternate model for thermonuclear supernovae

Thermonuclear supernovae

A very different kind of supernova results from a terminal evolutionary phase of compact white dwarfs in binary systems (Fig 2.6 and Nomoto et al., 1997, Thielemann et al., 1986). Accretion of further material from the secondary onto the white dwarf eventually ends up in conditions which ignite carbon inside the white dwarf, which in such a degenerate environment results in a runaway explosion with total disruption of the star. Generally no hydrogen envelope is present; therefore these supernovae are called 'Type Ia'.

We distinguish several scenarios from either the progenitor evolution or the trigger of carbon ignition. Progenitors may be relatively massive white dwarfs with a nondegenerate companion star in its high-mass loss phase ('single-degenerate'). In this case, the accreted hydrogen burns steadily, increasing the white dwarf density gradually above the carbon ignition density ('Chandrasekhar models'). Alternatively, the accretion onto a 0.6–0.9 $M_\odot$ carbon–oxygen white dwarf gradually accumulates a shell of helium, which eventually becomes massive (0.15–0.20 $M_\odot$) and hot enough to ignite; the compression shock wave from this helium flash then may ignite carbon at the center of the white dwarf ('sub-Chandrasekhar' or 'helium cap' models). In both these models, accretion occurs at relatively high rates (10^{-8}–10^{-6} $M_\odot$ yr^{-1}), resulting in steady hydrogen burning (rather than accumulation as in the case of novae). 'Supersoft' X-ray emission ($\leq$keV) may result from these progenitors, from nuclear burning heating the white-dwarf surface to unusually high temperatures; this could help us to recognize candidates for future thermonuclear supernovae. Note that the state of the companion determines how the mass transfer occurs. An AGB star companion with its strong wind might engulf the white dwarf, remeniscent of symbiotic stars; alternatively, Roche-lobe mass transfer might occur, in a cataclysmic system. Also, hydrogen burning could be avoided if the companion is a helium star already deprived of its H envelope in earlier binary evolution. A third class of models has two white dwarfs in a close-orbit binary system ('double-degenerate'or 'merger' models). Gravitational radiation incurs loss of orbital energy and eventually leads to merging of the two white dwarfs. The resulting object generally exceeds the Chandrasekhar stability limit and ignites carbon, as above. Rotation and strong tidal effects add special characteristics to this scenario, as does the specific composition of the igniting material.

In all three cases, the compactness of the fuel and the high thermal conductivity of the white-dwarf matter result in a runaway-type evolution, where the nuclear energy generation rate is too high for any adjustment processes: nuclear burning proceeds up to the iron peak, and the enormous energy density disrupts the entire star in a gigantic explosion. The nucleosynthesis conditions in this type of supernova are very different than for core collapse: nuclear burning occurs simultaneously with neutronization of matter, and the temperatures and densities most likely induce NSE. A large amount of radioactive ^{56}Ni (0.5 to 1 $M_\odot$) may be produced. Details of the supernova flame evolution determine the evolution of the light curve and the velocity profile of the ashes; a critical parameter is the duration of the subsonic deflagration phase relative to the supersonic detonation phase of the burning front. The abundances of neutron-rich isotopes of the iron group may provide sensitive diagnostics of this phase. Physical models of this phase of the supernova have not been obvious, although flame propagation in combustion engines shows promising similarities in details (Niemeyer, 1999). In empirical full-scale models, parameters are tuned to the observed appearance of

the supernovae; the empirical 'W7' model still serves as the best description (Iwamoto et al., 1999). Nevertheless, the evaluated total bolometric light for this class of supernovae has been found to be identical to within a few percent and forms the basis of the use of Type Ia supernovae as standard candles in cosmological studies (Branch, 1998). The absence of an outer envelope implies that both the overall radioactivity produced and the nucleosynthesis abundance pattern are dominated by the white-dwarf configuration, which is hence expected to vary less than the core-collapse supernovae, which are the final stage for stars of masses between 8 and $\sim$80 $M_\odot$.

Supernova Gamma-Rays

From their very different progenitors, core-collapse supernovae are expected to be found wherever massive stars form, with a relatively short time lag after initial star formation due to the short (million years) evolutionary time scale of such stars. On the other hand, thermonuclear supernovae occur only after intermediate-mass stars have terminated their stellar evolution ($\sim 10^8$ yr and more), and the remaining white dwarf within a binary system accumulates a critical surface layer from its companion.

How do γ-ray-emitting radioisotopes relate to these two supernova types? The large amounts of ^{56}Ni and ^{57}Ni radioactivity ($\sim$0.5 $M_\odot$ for thermonuclear, about 1/10 of that for core-collapse supernovae) provide the prime γ-ray diagnostics of the explosion morphology: when the supernova envelope gradually becomes transparent to γ-rays, decay γ-rays show up as a line feature above the Compton-scattered continuum γ-ray emission. Different relative γ-ray line intensities, as they evolve with time, encode the structure of the envelope and its mixing with fresh nucleosynthesis products. Gamma-ray line shapes measure the nucleosynthesis ejecta velocities, complementing the velocity information of atomic lines from the envelope [here ^{44}Ti adds late lightcurve information to the early lightcurve data from Ni isotopes (Chan and Lingenfelter, 1991)]. The unique information from γ-ray measurements is a calibration of the total radioactivity produced in the event and powering the light curve after the initial flash in all spectral bands. The Ni isotopes again address the early light curve, where abundant optical/UV/IR light curves need such calibration; the ^{44}Ti information is unique for the late supernova/early supernova remnant phase which is difficult to constrain otherwise. Additionally, the yields in the specific isotopes which are directly visible through γ-rays set constraints on the nucleosynthesis conditions and inner explosion dynamics (this adds ^{26}Al and ^{60}Fe to the list of relevant γ-ray probes of supernovae).

Novae

A classical nova is now understood to result from explosive burning of a shell of hydrogen which has been accreted onto a white dwarf from a companion

star. This evolutionary path is reminiscent of the mass transfer path to a thermonuclear supernova (see Fig 2.6). The rate of accretion must be tuned within a range $\leq 10^{-9}$ $M_\odot$ yr^{-1}, such that the gravitational energy release of the accretion flow remains below the critical heating towards hydrogen nuclear burning on the white-dwarf surface. On the other hand, accretion must be sufficiently rapid to build up an amount of hydrogen which can trigger the nuclear burning that starts a nova, within the time scale of galactic evolution. Once the energy generation rate of nuclear burning rises above the level that can be radiated away by the white-dwarf surface, a runaway starts, raising the temperature rapidly to 10–100 million K and burning the entire hydrogen envelope within a few minutes (Gehrz et al., 1998). The violent convection triggered during this evolution dredges up some matter even from deeper layers of the white dwarf, mixing carbon, oxygen, and in some cases even heavier elements into the burning region. This results in nucleosynthesis under proton-rich, hot burning conditions, which leave behind a characteristic abundance pattern (José and Hernanz, 1997).

The details of nova nucleosynthesis are very hard to model; the short time scale of the event plus the criticality of convection for mixing fuels and determination of density and temperature of the burning region pose major challenges (Hernanz et al., 1997). Besides, the progenitor evolution is not understood, but determines the mass and composition of the underlying white dwarf (Kolb and Politano, 1997). Nevertheless, nuclear networks have been run under the conditions resulting from hydrodynamic evolution of novae, and have shown that intermediate-mass elements up to sulfur and silicon may readily be generated, consistent with the observed enrichments of such elements in the atmosphere of novae. Radioactivities important for γ-ray astronomy comprise a variety of β decaying species with relative short lifetimes, such as ^{19}F, ^{15}N, and ^{13}C. These are produced on the proton-rich side of the nuclear valley of Stability and hence decay through positron emission. This incurs intense nova γ-ray emission early on from positron annihilation, with a γ-ray energy of 511 keV. This 'annihilation flash' is of very short duration, so it can be observed only for the first day of the nova; therefore any detection would be fortuitous (Gomez-Gomar et al., 1998). On the other hand, substantial production of relatively short-lived ^{7}Be is expected to result in a γ-ray line at 478 keV, visible for months due to the 77 day decay time of this isotope. None of these radioactivities has been observed yet. Nevertheless, classical novae represent a site of nucleosynthesis with unique characteristics, and from chemical evolution studies we expect novae to be the main sources of the intermediate-mass elements neon, sulfur, and magnesium. Novae also are known to be significant dust producers and hence may deposit parts of their freshly produced elements onto dust grains, where they could be locked up and escape their discovery in the interstellar medium through their atomic radiation characteristics. There is however the prospect of more long-lived radioactivity generation from novae, which could be detected as diffuse γ-ray

line emission for years, or millions of years, after the nova. Novae which occur on very massive white dwarfs could be substantial producers of ^{22}Na, which with its decay time of 3.8 yr is an excellent candidate to be seen after the nova has settled.

10.3.3 Other Nucleosynthesis Sites

Other sites of nucleosynthesis, beyond stellar interiors and explosive events, will be described briefly below for completeness; they are less relevant to γ-ray studies of nucleosynthesis (Rohlfs and Rodney, 1988).

The Sun

Nucleosynthesis reactions inside the Sun provide the energy source that determines its structure and luminosity, but in a rather complex way. Therefore it remains difficult to convert external observations of solar parameters (e.g. those obtained from helioseismology) into constraints on the Sun's core nuclear physics environment. However the neutrinos produced as by-products of the hydrogen-burning reactions readily escape from the solar core. Major experiments have been performed or set up to record these, through chlorine, light-water Cherenkov, and gallium detectors (Kirsten, 1999). It is the deficit in several energy channels of ν's which provides the most sensitive test of nuclear processing in the solar interior. The large overlying gas column prevents diagnostics through γ-ray observations. Nevertheless, the Sun is a prominent source of γ-rays from nuclear excitations and continuum processes (see Chap 5).

Cosmic-Rays in Interstellar Space

The study of Galactic cosmic rays revealed an isotopic composition with lithium, beryllium, and boron elements greatly enriched with respect to standard abundances. Combined with the depression of these very elements in standard abundances, this is evidence that interstellar spallation occurs and contributes significantly to nucleosynthesis in the universe (Ramaty et al., 1999). Interstellar spallation nucleosynthesis for Li, Be, and B competes with $\alpha + \alpha$ reactions (for Li) and the neutrino process inside core-collapse supernovae (for ^{7}Li and ^{11}B), both being able to generate primary Li and B. For beryllium the spallation chain appears to be the predominant source, although the observational proof from low-metallicity stars remains difficult. Astration destroys some of these fragile elements.

Spallation reactions themselves are well understood; the interaction energies are well within the range of laboratory measurements, in the range above tens of MeV per nucleon. The relevance of this process in comparison to other nucleosynthesis channels is difficult to estimate, however, as the

most relevant low-energy cosmic-rays cannot be observed otherwise; hence their flux and energy spectra remain uncertain (see Chap 11).

Further proof of spallation nucleosynthesis in the interstellar medium exists from the direct measurements of the high-energy cosmic-ray composition with the Ulysses (Simpson and Connell, 1998) and Advanced Composition Explorer (ACE) (Stone et al., 1998) Instruments. Shortlived radioactive isotopes have been identified, such as ^{54}Mn, ^{10}Be, and ^{26}Al.

In order to estimate the global relevance of interstellar spallation nucleosynthesis for an isotope's abundance, a balance of the initial abundances and the source and destruction processes, a chemical evolution model including cosmic-ray propagation, is required.

More specifically, one may estimate the total nucleosynthetic yield for a nearby region of active massive star formation, such as the Orion region. It was found, however, that even in this favorable case the yield of a relatively abundant hence γ-ray-bright isotope such as ^{26}Al still remains below instrumental sensitivity limits.

In the solar system, enrichment of meteoritic samples in ^{26}Mg had been a striking puzzle for a long time (MacPherson et al., 1995). Some of the models to explain this enrichment invoke injection from a nearby nucleosynthetic event just before the formation of the solar nebula. Any γ-ray-emitting radioactivity would have decayed since then, however. Other models invoke local production through cosmic-ray interactions (Shu et al., 1987).

The Big Bang and the Early Universe

The early universe's evolution is commonly described by expansion from a hot Big Bang singularity. Initial global thermal equilibrium involves all possible states of matter; the high temperature and density maintains a thermal distribution throughout; and strong, weak, and electromagnetic reactions equilibrate all system components more rapidly than the global system evolves. This initial fireball expands rapidly. Nuclei begin to form when the temperature drops below the regime of nuclear binding energies ($\simeq$8 MeV). At this time, the density of baryons has fallen to 10 g cm^{-3}, however, and rapid expansion soon constrains the nuclear reaction rate due to a lack of collisions. Hence the period of primordial nucleosynthesis is bounded from two sides, and it encompasses universe ages from 0.01 to 200 s.

Big Bang nucleosynthesis manifests itself in the primordial abundances of four species: the abundances of ^{4}He, D, ^{3}He, and ^{7}Li can all be expressed as a function of the universe's photon-to-baryon ratio (Schramm and Turner, 1998). The relation of these abundances to the key cosmological parameters implies that our present understanding of the early universe is intimately coupled with our understanding of nucleosynthesis.

There are no γ-ray-emitting radioactive species left over from this early nucleosynthesis. The primordial composition, or at least an approximation

of it, is conserved in the first generation of stars and in the gas that we can probe at very large redshifts ($z \simeq 4$) with quasar absorption lines.

10.4 Gamma-Ray Lessons on Supernovae

10.4.1 Individual Nucleosynthesis Sources

Thermonuclear Supernovae

A goal for γ-ray astronomy for the last three decades has been the detection of characteristic lines from the decay of radioactive ^{56}Ni and its daughter ^{56}Co, produced in supernovae. Type Ia events are favored over the other supernova classes because they produce an order of magnitude more ^{56}Ni than the other types ($\sim$0.6 $M_\odot$), and they expand rapidly enough to allow the γ-rays to escape before all the fresh radioactivity has decayed. Even so, detection of these events has been difficult to achieve.

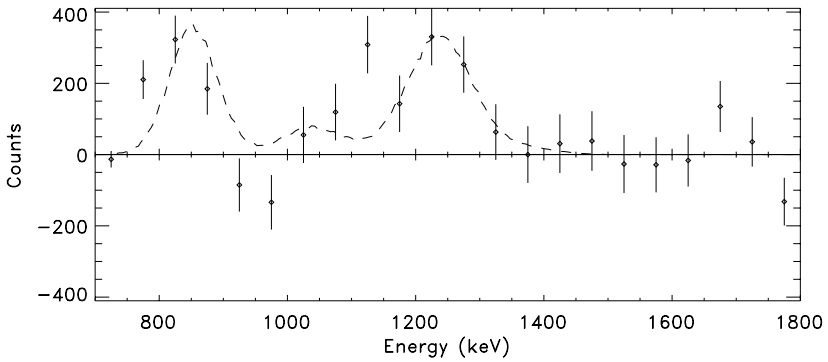

Fig. 10.7. SN 1991T spectrum as measured by COMPTEL, after subtraction of a background model. Reproduced with permission from Morris et al. 1995

The only Type Ia supernova which has possibly been seen in γ-rays is SN 1991T in the galaxy NGC 4527. This galaxy is $\sim$17 Mpc away (determined from Cepheid variables), and in the direction of the Virgo cluster. The supernova was unusually bright at maximum (0.7 $M_\odot$ of ^{56}Ni) and the light curve evolution was unusually slow. The classification as a peculiar Type Ia event is based on the absence of the silicon lines so typical in early Type Ia spectra. In addition, the Fe III lines were unusually strong at early epochs. Since no other iron group lines were observed at this time, this iron was probably not a fresh nucleosynthetic product. The spectra became more typical of Type Ia events at later epochs, when the expanding debris became more transparent. Detection of high velocity ($\sim$13 000 km s^{-1}) iron and nickel in the outer

layers of SN 1991T favors models where the subsonic flame front propagates to larger distances from the white-dwarf core before making the transition to a detonation. These types of delayed-detonation models are also consistent with the velocity profile of most of the other ejecta (silicon, calcium) seen in SN 1991T. Detection of the 812 keV γ-ray line from the decay of ^{56}Ni in the early light curve would have been direct evidence for a delayed detonation, as the line cannot be seen when the ^{56}Ni is embedded deeper in other categories of Type Ia models, which have been discussed for SN 1991T as well. These models may be favorable for ejecting a larger than average ^{56}Ni mass, and seek to explain some of the other early light curve peculiarities as arising from interactions of the supernova debris with the thick disk of material which surrounded the merger.

The tentative detection by the COMPTEL Compton telescope (Morris et al., 1995) of the ^{56}Co decay γ-rays (Fig 2.7), at 3–4σ significance only suggests that this isotope was present in the outer envelope and supports extensive-mixing scenarios. The COMPTEL flux value converts into an overly large ^{56}Ni mass, between 1.3 $M_\odot$ (for a distance of 13 Mpc) and 2.3 $M_\odot$, the value for the 17 Mpc favored currently. This would require that almost all of the Chandrasekhar-mass white dwarf must have turned into radioactive ^{56}Ni. Upper limits from OSSE (Oriented Scintillation Spectrometer Experiment on the Compton Obseervatory) may indicate that the COMPTEL ^{56}Co line flux is too high.

SN 1998bu at only 8–11 Mpc distance was observed by the CGRO instruments for several months. Apparently it occurred deeper within its host galaxy, M96, as inferred from apparently local reddening. Appearing rather 'normal' from its light curve and spectra, the ^{56}Ni γ-ray lines seem dimmer than expectations, however neither OSSE (priv. communication) nor COMPTEL (Georgii et al., 2000) have seen any of the ^{56}Ni decay chain γ-ray lines.

Rapid pointing of γ-ray telescopes at early times after the supernova is essential for proof/disproof of the helium cap models. INTEGRAL's spectrometer with its superior sensitivity would be able to add line shape (hence velocity) information for further diagnostics; note however that for broad lines the sensitivity of high-resolution instruments degrades. More detections of Type Ia supernovae in ^{56}Ni are required to clarify how typical SN 1991T was.

Type Ia supernovae of a rare sub-type could be important sources of ^{44}Ti. Predicted ^{44}Ti yields for sub-Chandrasekhar models (Tutukov et al., 1992) are 200–3000 times the relative solar ^{44}Ca proportion. Depending on how frequently these sub-Chandrasekhar mass white dwarfs explode, these large production factors open the possibility that these types of thermonuclear supernovae might be the principal source of ^{44}Ca, rather than the typical core-collapse event. The ^{44}Ti observation from Cas A, generally believed to be a core-collapse supernova, presents a counterexample of a ^{44}Ti source, however.

Gravitational-Collapse Supernovae

Core-collapse supernovae of Type Ib synthesize 5 to 10 times less ^{56}Ni than a typical Type Ia supernova, but expand almost as rapidly. Thus their early γ-ray signal should be intermediate between Type II and Type Ia. Any Ni or Co γ-ray line detection of a Type II supernova outside the Local Group is very improbable with present instruments.

The best studied supernova of all is the Type II supernova SN 1987A, (see Fig 2.8) mainly because of its proximity, but also because instrumentation in IR to γ-ray regimes had matured and were for such observations (Phillips et al., 2000). Detection of ^{56}Co and ^{57}Co lines from SN 1987A by many experiments provided the first extragalactic γ-ray line signal from radioactive isotopes (Gehrels et al., 1988). The early appearance of ^{56}Co γ radiation presented evidence for enhanced mixing of supernova products within the envelope.

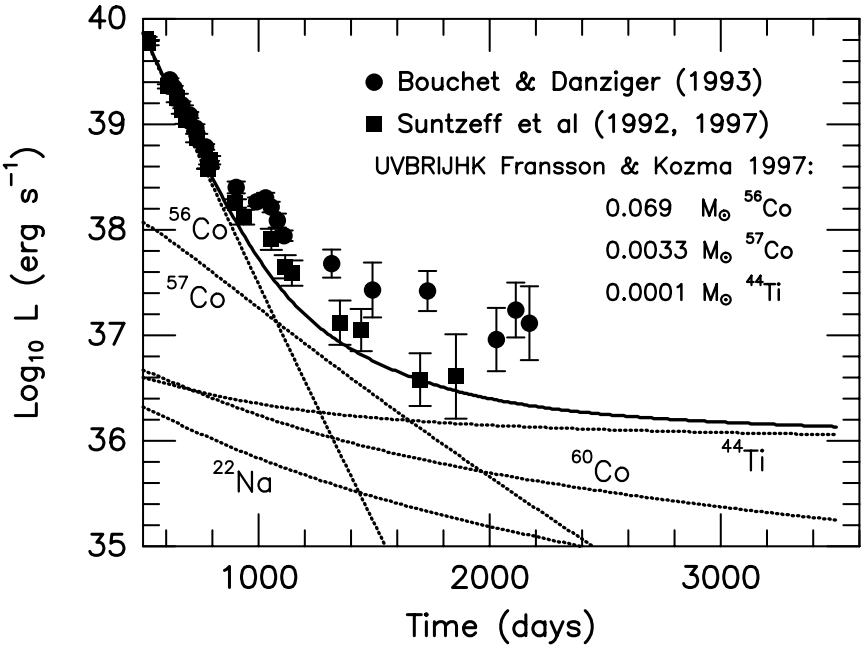

Fig. 10.8. The light curve of SN 1987A. The optical/UV emission is found to be consistent with energy input from the radioactivities seen in γ-rays, as indicated by the reference lines for ^{56}Co and ^{57}Co; ^{44}Ti energy input is also shown. Reproduced with permission from Diehl and Timmes 1998.

Later, OSSE reported detection of ^{57}Co radiation from SN 1987A, with a measured flux of $\sim 10^{-4}$ photons cm^{-2} s^{-1} between 50 and 136 keV (Kurfess

et al., 1992). For models with low ^{57}Co optical depths, the observed γ-ray flux suggested that the ^{57}Ni/^{56}Ni ratio produced by the supernova was about 1.5–2.0 times the solar system ratio of ^{57}Fe/^{56}Fe. Estimates of SN 1987A's bolometric luminosity at optical and infrared wavelengths beyond day 2000 show that the cooling time of the remnant is longer than previously thought ($\leq$1 magnitude per 1000 days). Fits of cooling models to these light curves yield 0.069 $M_\odot$ of ^{56}Co and 0.0033 $M_\odot$ of ^{57}Co, and hence a ^{57}Ni/^{56}Ni ratio in reasonable agreement with the γ-ray measurements.

If we exclude any energy input from a pulsar, an accreting compact object, or circumstellar interaction, SN 1987A is now in a phase where the dominant energy source should be from the decay of ^{44}Ti (see Fig 2.8). Its thermal luminosity should derive mostly from e^+ kinetic energy. From the late-time bolometric light curves 10^{-4} $M_\odot$ of ^{44}Ti is suggested. The type of energy input may be difficult to resolve uniquely, however, if the atomic processes that convert energy from radioactivity into optical/infrared radiation are no longer in steady state.

For a distance of 50 kpc to SN 1987A and a ^{44}Ti e-folding lifetime of 89 yr, 1×10^{-4} $M_\odot$ of ^{44}Ti would produce a γ-ray line flux of 2×10^{-6} photons cm^{-2} s^{-1}. This line flux is too small for the instruments aboard CGRO, possibly achievable for INTEGRAL, ESA's International Gamma-Ray Astrophysics Laboratory to be launched in2002. Spherically symmetric models of SN 1987A suggest ^{44}Ti ejection at very low velocities ($\leq$1000 km s^{-1}), and hence a very narrow γ-ray line. On the other hand, broad infrared lines of nickel, early appearance of X-rays, and smoothness of the bolometric light curve argue for mixing of ^{56}Ni out to velocities between 2000 and 4000 km s^{-1}. With ^{44}Ti and ^{56}Ni originating from similar processes, it will be interesting to measure the line shapes, in order to obtain valuable information about the explosion mechanism and multi-dimensional mixing.

The Cas A supernova remnant in our Galaxy is relatively close ($\simeq$3.4 kpc), young (explosion in 1668−1680), and accessible (physical diameter $\sim$4 pc, corresponding to an angular extent of $\sim$4 arc min), making it one of the prime sites for studying the spatial structure and kinematics of a supernova remnant as it ploughs into the interstellar medium. Cas A exhibits a rich variety of phenomena: fast-moving knots have been diagnosed as ejecta clumps from the supernova explosion, and jet-like structures also support spherical non-symmetry. The discovery of the central compact object with the Chandra X-ray telescope, plus the signs of an intense pre-supernova wind in quasistellar flocculi on the outside, support the classification as a Type Ib event from a massive progenitor. The COMPTEL discovery of 1.157 MeV γ-rays from the $\sim$ 300 yr old Cas A supernova remnant (Fig 2.9) (Iyudin et al., 1994) was a scientific surprise. Supernova models had indicated that $\sim3\times10^{-5}$ $M_\odot$ of ^{44}Ti would be ejected (Timmes et al., 1996), which translates into a γ-ray intensity generally below instrument flux sensitivities. COMPTEL's detection of Cas A at ~3 $(\pm1)\times10^{-5}$ photons cm^{-2} s^{-1} in the 1.157 MeV line, implies

(1–2)$\times 10^{-4}$ $M_\odot$ of ^{44}Ti. Conversion of the measured flux into mass limits must account for the uncertainties in the ^{44}Ti lifetime, the distance to the event, and the precise time of the explosion as well as a possible underlying γ-ray continuum from electrons accelerated in the remnant. Ionization-delayed radioactive decay has been proposed as a potential observational bias, but is probably unimportant.[14]

The abundance of ^{44}Ti and ^{56}Ni as a function of mass inside a 25 $M_\odot$ star, shown in Fig 2.5 for a standard model, suggests that if ^{44}Ti is ejected ejection of ^{56}Ni is needed too and produces a bright supernova. If interstellar absorption did not attenuate the optical light curve, the Cas A supernova would have had a peak apparent magnitude of $m_V = -4$, easily recognizable in the sky. Cas A was not widely reported as such; some 10 magnitudes of visual extinction is required to make the γ-ray ^{44}Ti measurements consistent with these (absent, except for one hint) historical records.

There may indeed have been such a large visual extinction to Cas A at the time of the explosion (Hartmann et al., 1997): if Cas A was embedded in a dusty region, or experienced significant mass loss which condensed into dust grains before the explosion, the extinction could have been exceptionally large but not observed. Measurements of the X-ray scattering halo around Cas A with ROSAT (Röntgen Satellite) and ASCA (Advanced Satellite for Cosmology and Astrophysics) suggest an unusually large reddening correction. The X-ray scattering halo is unusually low for the derived N_H values ($N_H = 1.8\times 10^{22}$ cm^{-2}), while this N_H is twice as large as what $A_V = 5$ usually implies. Extra material seems to be distributed close to Cas A, possibly the dusty shell of material ejected prior to the explosion as a Type Ib supernova. The supernova shock wave could have destroyed much of the dust as it propagated through the debris and the material surrounding the Cas A supernova. This scenario would be consistent overall, with the lack of optical detection, excess neutral hydrogen column density, dust-free and metal-rich debris, and ejection[15] of $\sim 10^{-4}$ $M_\odot$ of ^{44}Ti.

Notice that $\sim 10^{-4}$ $M_\odot$ of ^{44}Ti is inferred to have been ejected both in SN 1987A (a Type II event) and in Cas A (probably a Type Ib event). This agreement may be fortuitous; however it may suggest that the inner core-collapse explosion/accretion mechanism is well regulated.

The COMPTEL search for ^{44}Ti sources in the Galaxy did not discover as many sources as would be suggested by a Galactic core-collapse supernova rate of about one event in even 30 yr (Dupraz et al., 1997; The et al., 2000).

[14] Ionization by the supernova reverse shock requires major parts of ^{44}Ti ejecta to remain in rather dense clumps (Mochizuki et al., 1999).

[15] ^{44}Ti yields may be enhanced relative to ^{56}Ni by explosion asymmetries or yet-unknown details of fall-back and mass accretion onto the compact remnant. The decay chain of ^{44}Ti involves electron capture and hence may be inhibited by highly ionized nucleosynthesis ejecta in the early remnant phase (Mochizuki et al., 1999).

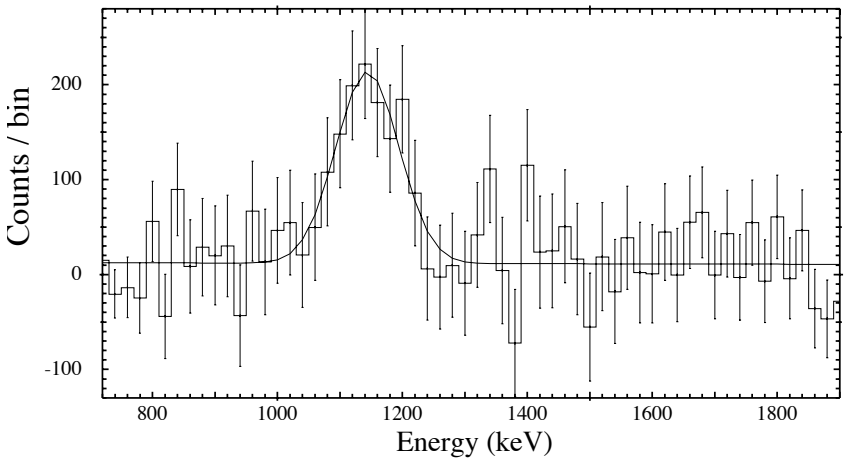

Fig. 10.9. The COMPTEL discovery of Cas A in the γ-ray line of ^{44}Ti demonstrates that nucleosynthesis products from the inner region of core-collapse supernovae may be ejected into the interstellar medium. Reproduced with permission from Diehl and Timmes 1998

This suggests that ^{44}Ti-producing supernovae are exceptional events. Cas A appears to be one. ROSAT X-ray measurements had revealed another supernova remnant, RX J0852.0-4622 of diameter 2°, superimposed on the

7° diameter Vela supernova remnant (Aschenbach, 1998); COMPTEL may have discovered ^{44}Ti γ-rays from this source, which would place it very nearby at a distance of 200 pc only (Iyudin et al., 1998). This case illustrates the new potential of ^{44}Ti γ-ray observations to search for supernova remnants in otherwise difficult if not totally inaccessible regions.[16] Indeed, for very nearby sources ($d \leq 500$ pc) their ^{26}Al emission should be detectable individually, and thus a comparison of ^{44}Ti and ^{26}Al yields alone allows age and distance determination for such objects. Future observation/instruments may make this a realistic proposition.

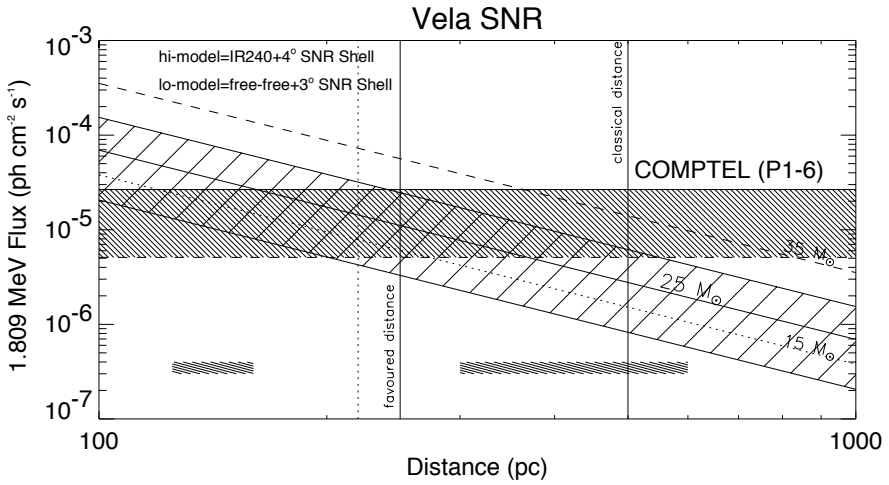

Fig. 10.10. The residual 1.809 MeV signal attributed to the Vela supernova remnant appears consistent with core-collapse supernova models, in particular if a distance of ∼250 pc is assumed

From the initial COMPTEL discovery of ^{26}Al emission from the Vela region there was some hope to detect ^{26}Al from one single source, the nearby Vela supernova remnant. Refined analysis showed, however, that the main 1.809 MeV feature in this region is significantly offset from the Vela supernova remnant (see Fig 2.12 left). The offset may be due to a contribution from the RX J0852.0-4622 supernova remnant (Aschenbach et al., 1999) and/or from the known populations of OB associations and active star-forming regions in this direction at larger distances (Diehl et al., 1999). A direct calibration of core-collapse supernova ^{26}Al nucleosynthesis on the Vela SNR, however, does not apply, and model predictions are consistent with the flux range seen

[16] Either confused other structures, or occulted in cases of supernovae occurring inside dense cloud regions.

by COMPTEL (see Fig 2.10). Note that the distance to this SNR has been revised from the traditional 500 pc to ∼250 pc.

Novae

The origin and evolution of an accreting white dwarf which becomes a classical nova are essentially unknown, and yet have important consequences for any γ-ray signal which may originate from novae (Gomez-Gomar et al., 1998). For example, the composition of the nuclear burning region is often assumed to be a 50–50 mixture of accreted material and dredged-up white-dwarf material. Typically the accreted material is taken to have a solar composition, and the white dwarf material is assumed to be an oxygen–neon–magnesium mixture in mass proportions of 0.3:0.5:0.2; however oxygen–neon–magnesium ratios of 0.5:0.3:0.05 have been suggested from evolutionary models as more appropriate (Ritossa et al., 1996), although the detailed abundances could vary substantially with initial stellar mass. Since the yield of ^{26}Al and ^{22}Na from novae is sensitive to the initial ^{25}Mg and ^{20}Ne abundances, this latter white-dwarf composition eliminates most of the necessary seed material from which radioactive isotopes may be synthesized. Uncertainty in binary-star evolution and the binary mass distribution function correspond to uncertainty in the fraction of classical novae that originate from $\geq$8 $M_\odot$ main-sequence stars.

All nova models predict ejected masses that are by an order of magnitude too small when compared to observations. As the white dwarf becomes more massive, less material is accreted before the fuel ignites and the total mass of matter lifted to escape velocity, ^{22}Na and ^{26}Al in particular, is smaller. If the inconsistency between model and observed ejected masses is resolved by resorting to a less massive ($M \leq 1.1\ M_\odot$) white dwarf, then the ^{26}Al yields are expected to increase due to the lower burning temperatures. However, should a more violent explosion be required, and be achieved by increased mixing of core material, then the higher burning temperatures are expected to decrease the ^{26}Al mass ejected. While these examples show that our understanding of the physics is rather incomplete, the thermonuclear runaway model for classical novae has been a success of the first order. A nova event within 1 kpc would provide several important diagnostics (radioactive and otherwise) for refining the mixing and energetics aspects of the model.

Observationally, about 1/3 of the nearby novae which could be analyzed in detail have been found to show large enhancements in the abundance of neon, among other intermediate-mass elements. This has been taken as evidence that these novae occurred on white dwarfs with substantial enrichment in elements heavier than oxygen (thus attributed either to more massive progenitors or to a self-enrichment through successive and frequent surface nucleosynthesis events). From neon seed nuclei, ^{20}Ne(p,γ) and successive proton capture reactions can occur in the hot hydrogen-burning environment, to

produce substantial amounts of ^{22}Na. Note however that the high temperatures required for efficient ^{22}Na production makes only the upper end of the white-dwarf mass spectrum ($\geq$1 M$_\odot$) relevant for ^{22}Na production. For these massive white dwarfs, the amount of accreted material needed to trigger the nova is less, and it is still unclear how the observed large ejected masses from neon-rich novae should be understood. Therefore upper limits on the ^{22}Na yields per novae are interesting, even in the absence of any detection: the flux limit in the 1.275 MeV line of $\sim 3\times10^{-5}$photons cm^{-2} s^{-1} corresponds to $\sim4\times10^{-8}$ M$_\odot$ of ^{22}Na, if all individual limits are combined (Iyudin et al., 1995). Current models for more massive white-dwarf novae still predict values about an order of magnitude lower, though [e.g., 1.6×10^{-9} M$_\odot$ for a 1.25 M$_\odot$white dwarf (José and Hernanz, 1997)].

For the progenitor range considerably below 1 M$_\odot$, production of ^{26}Al should be enhanced, because burning occurs at lower temperatures and is less violent, photodestruction of the freshly produced ^{26}Al is avoided. Some models predict enrichments of the ^{26}Al isotope with respect to stable ^{27}Al of up to 10^{-3}, which, combined with observed ejected masses of a few 10^{-4} M$_\odot$, could accumulate to a significant part of the observed diffuse glow of ^{26}Al emission from the Galaxy (see below). However this naive argument already outlines the difficulty in such estimates: no self-consistent evolutionary model has been carried through to predict the amount of Galactic ^{26}Al from such novae. Rather, specific models of nucleosynthesis have been calculated, often selecting the most favorable conditions. The fractional enrichments obtained have then been adjusted to the observed ejected masses, which are generally about one order of magnitude higher than those produced in standard models. The reason for this discrepancy is not understood. Moreover, such nucleosynthesis production for the modelled progenitor then is multiplied by an uncertain fraction of novae occurring on relatively massive white dwarfs (the mean white dwarf mass lies in the vicinity of 0.4–0.5 M$_\odot$). Only about a dozen novae have been observed with adequate spectroscopic data to determine atmospheric abundances; the values for the latter are uncertain due to the atmospheric excitation model that underlies interpretation of spectroscopic data in terms of elemental abundances. These dozen novae all are 'disk novae' at distances within a few kpc, hence not representing the Galactic Bulge. Any Galactic nova population estimate therefore must make assumptions about nova frequencies per class in the disk and bulge, mostly taken from observations of nearby galaxies such as M31 and the Large Magellanic Cloud. Obviously, there are substantial open issues. Gamma-ray line observations would be a paramount tool to help clarify these. Nova Velorum 1999 at a distance of 0.8–2 kpc could be another opportunity; it was observed by CGRO instruments at the time this article was being written. Diagnostics in the 511 keV annihilation line and the 478 keV line from ^{7}Be await detection (Harris et al., 1991).

Stellar Interiors: Hydrostatic Nuclear Burning

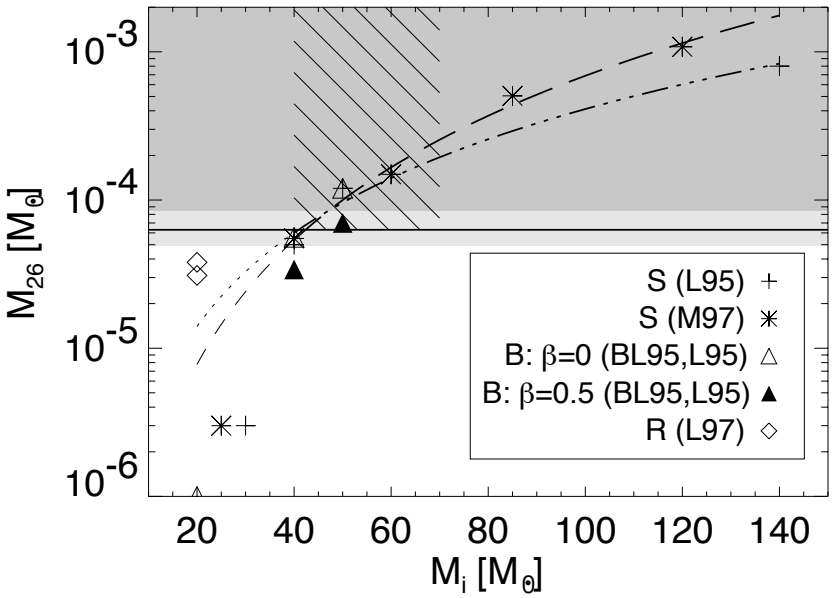

Fig. 10.11. The expected production of a WR star exceeds the sensitivity limit of COMPTEL's 1.8 MeV survey: the special conditions of the γ^2Velorum binary system and its current phase must be invoked to explain the absence of an 1.809 MeV signal from a WR star at this distance

At present, sensitivity levels of γ-ray telescopes identify only one massive star as a candidate source: the γ^2Velorum system in the Vela region at a distance of 260 pc. Indeed, this O-star/WR star binary system has been studied in great detail, but ^{26}Al emission at the level predicted by models is not observed (Oberlack et al., 1999) (see Fig 2.11). Modification of the ^{26}Al ejected from WR11 due to the O star companion and an age of WR11 beyond its maximum ^{26}Al ejection phase are possible explanations of the discrepancy.

10.4.2 Integrated Nucleosynthesis

^{26}Al in the Galaxy

^{26}Al with its radioactive decay time of 1.04×10^6yr accumulates in the interstellar medium from many individual sources of nucleosynthesis. This results in a diffuse glow of active regions of nucleosynthesis in the Galaxy in the 1.809 MeV γ-ray line, imaged for the first time with the COMPTEL telescope (Diehl et al., 1995). Since the pioneering discovery in 1982 by HEAO-C, the third High-Energy Astronomy Observatory Satellite of NASA , many

experiments have contributed to aspects of ^{26}Al astronomy, as summarized in a recent review (Prantzos and Diehl, 1996). Instrumental capabilities differ substantially, but the integrated flux measured from the general direction of the inner Galaxy, integrated over latitude and the inner radian in longitude, has been used to roughly compare results. All measurements are consistent with values of 4×10^{-4} photons cm^{-2}s^{-1}. Note that the determination method varies between instruments, and in particular the flux values for the nonimaging instruments depend on the assumed spatial distribution: nonimaging instruments essentially assume the same (or equivalent) smooth spatial distribution narrowly following the plane of the Galaxy as had been derived from COS-B measurements of Galactic continuum γ-rays in the $\geq$100 MeV regime.

The distribution of 1.809 MeV emission seems significantly different from the continuum, however (see Chap 4). Images derived from COMPTEL measurements show spatial structure in the emission. The ridge of the Galactic plane dominates; however there is asymmetry in the emission profile along the disk, with several prominent regions of emission, such as in the Vela region and Cygnus regions. All estimates of the absolute ^{26}Al mass in the Galaxy rest on assumptions about the spatial distribution of the sources, as the 1.809 MeV measurements themselves do not carry distance information. The COMPTEL team fitted a wide range of models for candidate source spatial distributions to their high-quality imaging data (over 30σ significance) (Knödlseder et al., 1999b). When localized regions of emission beyond the inner Galaxy are excluded, then all axisymmetric model fits yield a Galactic ^{26}Al mass of $\sim$2 M$_\odot$. The extent of spiral-arm emission can be estimated if a composite model of disk emission plus emission along spiral arms is adopted and compared to the disk-only model. Spiral structure appears significant, contributing between 1.1 M$_\odot$ and all of the ^{26}Al.

If massive stars are the candidate sources, they should follow the molecular gas distribution, and thus would be traced by CO survey data. Although generally compatible with the ^{26}Al map, other tracers were found to provide a better fit. One of these tracers is free electrons from ionizing effects related to nucleosynthesis sources. One may estimate the free-electron content of the interstellar medium from radio measurements of free–free emission, which can be obtained after subtraction of synchrotron emission. Alternatively, a semi-analytical model of spiral-arm structure based on HII region data, refined by free-electron measurements from pulsar signal dispersions, has been used. This tracer shows ridges similar to the ^{26}Al map at longitudes $\pm$35 degrees, along with a prominent feature in Carina (l = 280 degrees), and it is proportional to the 1.809 MeV map in all significant detail over the entire plane of the Galaxy. In particular, a calculation can reproduce the expected massive star population and the supernova rate from both maps consistently, if WR stars from high-metallicity regimes in the inner Galaxy provide the bulk of ^{26}Al (Knödlseder, 1999). Other good candidate tracers were identified

in warm dust maps, such as the long-wavelength maps from DIRBE (Diffuse Infrared Background Experiment) aboard the Cosmic Background Explorer (COBE) , or the far-infrared cooling lines at e.g. 158 μm from the ionized interstellar medium. All these arguments confirm that tracers which measure the energy input into the interstellar medium from massive stars appear to represent an approximate representation of the ^{26}Al source distribution.

The evidence above may be taken to constrain ^{26}Al contributions from classical novae, where a smooth distribution of the emission with a pronounced peak in the central bulge region would be expected. The upper limit for such contributions is probably 1 $M_\odot$ of ^{26}Al. On the other hand, Ne-rich novae in our Galaxy may occur more frequently in the disk, and hence follow the Galactic distribution of massive stars more closely than the overall white-dwarf distribution. In this case, differentiating nova sources from massive star sources will rely on the consistency of the calculated yields with other lines of evidence (such as other radioactive isotopes), supplemented by 1.809 MeV line shape arguments.

More local ^{26}Al contributions may play a significant role: the slightly lower ^{26}Al flux value from COMPTEL is mainly based on Galactic-plane emission, while the large field-of-view instruments (100–160 degrees) of GRIS (Gamma-Ray Imaging Spectrometer) and SMM (Solar Maximum Mission) mainly sampled the sky along the plane of the ecliptic with relatively more exposure of the high-latitude sky; those instruments may include large-scale flux of low surface brightness that COMPTEL's image failed to capture. ^{26}Al emission from the solar vicinity had been predicted long ago, but was discarded when COMPTEL's image showed dominant emission along the plane of the Galaxy. Local contributions to the overall emission are supported by the existence of two nearby pulsars at ∼100 pc distances (Geminga and R CrA), the nearby Gould Belt structure apparent in UV through young and massive B stars, and other massive-star activity signposts such as Loop I, which is associated with the nearby Sco–Cen association; all these suggest that the ∼500 pc environment of the sun may well have experienced a higher-than-average star formation and supernova activity during the past ∼50 million years. In view of the underlying continuum emission, and also very different instrumental techniques, each with substantial systematic uncertainties, the 1.809 MeV line flux measurements must be consolidated and ensured to be comparable before such speculations are further pursued.

Imaging of diffuse sources of MeV γ-rays is far from straightforward due to the high instrumental backgrounds and the complex γ-ray detection methods. Consistency checks between different techniques have shown that some of the spikyness of the apparent emission in the COMPTEL result could be an artifact of analysis techniques. Nevertheless, significant emission from the Cygnus, Carina, and Vela regions appears consolidated (Knödlseder et al., 1999b).

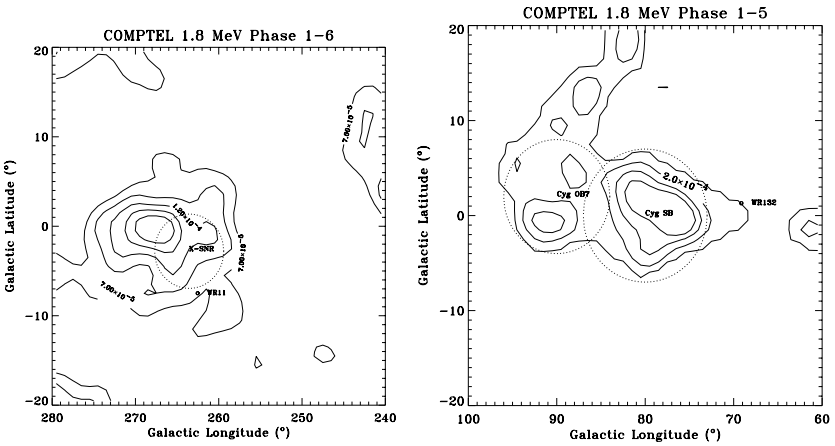

Fig. 10.12. Left: The Vela region image in the 1.8 MeV line from ^{26}Al shows no prominent emission from the nearest known candidate sources, the Vela supernova remnant and $\gamma^2 Velorum$. The peak of the emission rather coincides with several associations on the near side of the Vela molecular ridge, reflecting massive-star activity within these. Right: The Cygnus region 1.8 MeV image appears plausibly explained by the Cygnus superbubble and OB associations, the massive-star activity producing ^{26}Al

About 80% of the prominent 1.809 MeV emission associated with the Cygnus region (see Fig 2.12 right) can be understood in terms of the expected ^{26}Al signal from known sources (Del Rio et al., 1996). One may be puzzled by this high fraction, since ^{26}Al decays on a time scale longer than the observable features of supernova remnants and WR winds survive. It has been suggested that the ^{26}Al from this region attributed to'seen' sources should be multiplied by a factor of between 1 and 10 to account for'unseen' sources. COMPTEL images show structures which suggestively align with the Cygnus superbubble and the Cyg OB1 and OB2 associations. However is is difficult to spatially separate source regions, and in particular assess the significance of emission from the prominent group of WR stars in this region.

The Carina region (l = 282–295 degrees) presents a tangential view along a spiral arm, identified through a large molecular-cloud complex ∼2–5 kpc away, houses the prominent ≥140 $M_\odot$ star Eta Carinae (l = 288 degrees) and shows the densest concentration of young open clusters along the plane of the Galaxy. ^{26}Al production within these clusters as part of the Car OB1 association may relate to the observed 1.809 MeV feature at l = 286 degrees. This feature appears almost as a point source for the 4° resolution COMPTEL instrument, and thus may be spatially more confined than the expected signature from a tangential view into one of the Milky Way's spiral arms.

It is also interesting that some of the 1.809 MeV image structures which fail to align with spiral arms do coincide with directions towards nearby asso-

ciations of massive stars. Patchiness in such a nucleosynthetic snapshot might be expected from the clustering of formation environments of massive stars. If viewed from the outside, the Milky Way might also display the signs of massive star populations in the form of HII regions arranged like beads on a string along spiral arms, such as observed in M31 from H_α emission analysis, or in M51 from heated dust seen in infrared continuum at $\geq$15 μm. Interstellar absorption and source confusion prevents such mapping within the Milky Way. Therefore, detailed investigation of local systematic uncertainty in the COMPTEL image, that is, a quantitative limit to artificial bumpiness of the imaging algorithm, is important for such interpretation of 1.809 MeV emission. Similar concerns also apply to other instruments and future measurements of the morphology of Galactic nucleosynthesis radioactivity along the Galactic plane.

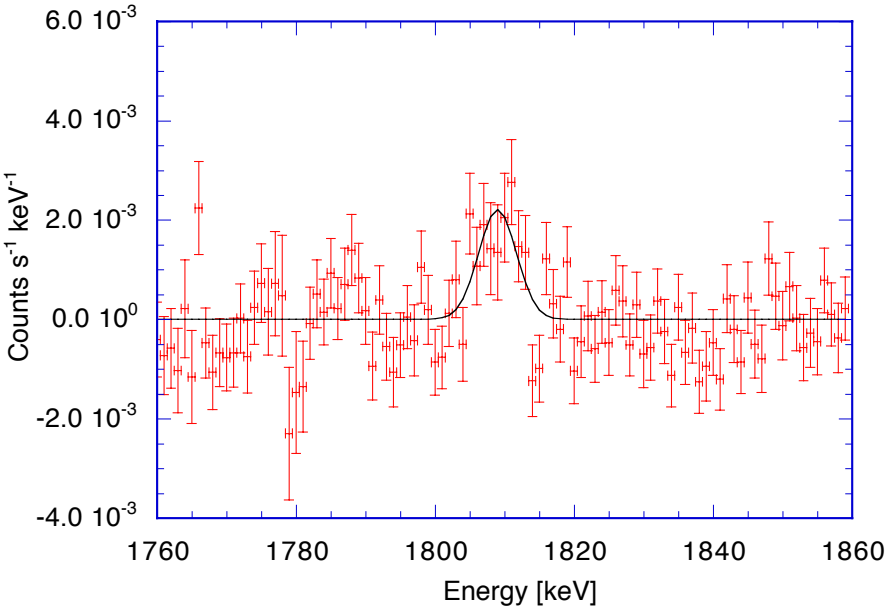

Fig. 10.13. The high-resolution study of the 1.809 MeV line from ^{26}Al may hold rich kinematic information about the source regions. Here the GRIS experiment reported significant line broadening, suggesting that ^{26}Al nuclei remain at high ($\sim$500 km s^{-1}) over 10^5 yr or more. (Reproduced with permission from Naya et al. 1996)

In a balloon flight, the GRIS Ge detector instrument ($\sim$3 keV energy resolution) drift scanned the Galactic-center region with its $\sim$100 degrees field of view, and detected the 1.809 MeV line at 7σ significance and a flux of 4.8×10^{-4} photons cm^{-2} s^{-1} (Naya et al., 1996). The main surprise in this measurement is the width of the line profile: it was significantly broader

than the instrumental resolution of the germanium detector and reported as $\Delta E = 5.4 \pm 1.4$ keV (Fig 2.13). This line width is much larger than expected from Galactic rotation ($\sim$1 keV), which again dominates above the broadening from random motions in the interstellar medium. It is presently difficult to understand how such high-velocity motion could be maintained over the million year time scale of ^{26}Al decay. Thermal broadening by a very hot phase of the interstellar medium ($\sim 10^8$ K) with long cooling times ($\sim 10^5$ yr) or a kinetic broadening at high average velocities ($\sim$500 km s^{-1}) seems to be required. Either case requires extremely low-density phases of the interstellar medium on large spatial scales. Alternatively one may hypothesize massive, high-speed dust grains as carriers of ^{26}Al to explain the measurement. This view derives some support from our current understanding of cosmic-ray acceleration. Further observations of the line shape are required to examine any spatial variations in the line broadening. A spectral resolution of $\sim$2 keV is required for such a study. Although the INTEGRAL mission may still have insufficient energy resolution to make complete velocity maps of the 1.809 MeV emission along the plane of the Galaxy, the brightest features can probably have their velocity centroids determined well enough to place them on the Galactic rotation curve and thus derive the distance to the features. Surveys which combine velocity information and Galactic latitude extent could then examine the existence and nature of any Galactic'fountains' and'chimneys' from possible 'venting' of ^{26}Al into the Galactic halo. The COMPTEL-measured latitude width may constrain the mean velocity of observed ^{26}Al below the GRIS value for an assumed young and hence narrow population of sources and isotropic expansion over 10^6 yr. In any case, the large line width measured by GRIS is inconsistent with the HEAO-C line width limit of $<$3 keV and needs confirmation, since it could have profound implications on our understanding of the interstellar medium in the Galaxy.

^{60}Fe in the Galaxy

Physically, ^{60}Fe should be a good discriminant of different source types generating ^{26}Al, because massive stars produce ^{26}Al and ^{60}Fe in the same regions and in roughly comparable amounts. While the ^{26}Al production occurs in the hydrogen shell and the oxygen–neon shell, ^{60}Fe is produced in He–shell burning and at the base of the oxygen–neon shell. Most important is that the bulk of both ^{26}Al and ^{60}Fe are produced, mainly during the presupernova evolution, at mass coordinates between 3 and 6 $M_\odot$ of typical $\sim$20 $M_\odot$ stars. These two isotopes should have similar spatial distributions after the explosion of these stars, if supernovae from massive stars dominate both ^{26}Al and ^{60}Fe nucleosynthesis.

An estimate for the injection rate into the Milky Way is the steady-state event rate times the average mass ejected per event; taking $M(^{26}\mathrm{Al}) \sim 10^{-4}$ $M_\odot$, $M(^{60}\mathrm{Fe}) \sim 4\times10^{-5}$ $M_\odot$, and $\sim$2 core-collapse supernovae per century, one obtains $\dot{M}(^{26}\mathrm{Al}) \sim 2.0$ $M_\odot$ Myr^{-1} and $\dot{M}(^{60}\mathrm{Fe}) \sim 0.8$ $M_\odot$Myr^{-1}. More refined

chemical evolution calculations suggest that Type II supernovae are responsible for a steady-state abundance of 2.2 ± 1.1 $M_\odot$ of ^{26}Al and 1.7 ± 0.9 $M_\odot$ of ^{60}Fe in the Galaxy, producing an intensity ratio in the decay γ-ray lines of ^{26}Al and ^{60}Fe of ∼16% (Timmes et al., 1995).

A few recent ^{60}Fe measurements and flux ratios with ^{26}Al have been obtained so far. SMM reported an upper limit of 8.1×10^{-5} photons cm^{-2} s^{-1} for the 1.173 MeV ^{60}Co line over the central radian of Galactic longitude, giving an upper limit of 1.7 $M_\odot$ of ^{60}Fe (Leising and Share, 1994).

From the GRIS balloon experiment, a more stringent upper limit of 17% has been derived on the ^{26}Al/^{60}Fe γ-ray line intensity ratio (Naya et al., 1998); this is confirmed by COMPTEL (Diehl et al., 1997). If this is the case, the initial model estimates for the total Galactic flux ratio might be too large. However, there are uncertainties of factors ∼2 in the models, from nuclear cross sections, explosion energy uncertainties (affecting the large ^{60}Fe contribution from explosive He-burning), and chemical evolution models.

Once ^{60}Fe can be detected with γ-ray telescopes, we can test the supernova origin of ^{26}Al hypothesis, since ^{60}Fe from other sources is negligible. [17]

Positrons in the Galaxy

Radioactive decays can generate positrons whenever the energy level of the daughter atom is below the energy level of the parent by more than the 1.022 MeV pair-production threshold. Interesting numbers of positrons are produced from the β^+ decay of ^{26}Al, ^{44}Ti, ^{56}Co, and the distinct nova products ^{13}N and ^{18}F. Annihilation produces two 511 keV photons if the positron and electron spins point in opposite directions or three photons in a continuous energy spectrum if the spins are parallel. The three-photon annihilation process usually involves formation of positronium, which then decays before being collisionally destroyed because of the low densities in interstellar space. As a result, the fraction of positronium radiation in the total annihilation signal carries information about the thermodynamic properties of the annihilation environment. A cold, neutral environment results in low positronium fractions and predominant annihilation in flight (Bussard et al., 1979), while larger positronium fractions tend to indicate annihilation in warmer environments, 5×10^3 K or hotter. The positrons produced by the interesting radioactive decays have average kinetic energies of ∼MeV, and thus are relativistic. Deceleration and thermalization are more likely than annihilation in-flight, so that the positron lifetime in interstellar space before annihilation is $\sim10^5$ yr (Chan and Lingenfelter, 1993). The thermalization process implies an intrinsically narrow 511 keV linewidth, which is related to the annihilation environment rather than to the positron production environment.

[17] Thermonuclear supernovae may be important sources, if neutron-rich nucleosynthesis happens in (supposedly rare) carbon deflagration supernovae (Woosley, 1997). In this case, a few ^{60}Fe hot spots from such events would be superimposed on the diffuse SNII ^{60}Fe glow.

In addition to annihilation from radioactive decays, positron annihilation is expected from the disks around accreting compact remnants, from the jets caused by dynamo action of accreting compact sources, and from γ–γ reactions in strong magnetic fields.

How can these various signals be differentiated? Positrons from radioactive decays usually annihilate in the diffuse interstellar medium where the thermalization lifetime is long. Positrons produced around compact objects should annihilate near the compact objects, since the density is usually much larger in those environments. This is expected to result in a more localized and possibly time variable signal. Such annihilation spectra may also contain such recognizable signatures as a high-energy tail above 511 keV from annihilation in-flight and/or bremsstrahlung, a blue-shift from positron jets moving towards the observer, a red-shift when originating from sources with a large gravitational field, or a distinctly smaller positronium fraction. Observations of the 511 keV line from positron annihilation show a steady diffuse component from the Galactic Disk, possibly superimposed upon a time-variable point source located near the Galactic Center reported in the 1980's (Ramaty et al., 1994). OSSE and SMM measurements of the annihilation radiation can be analyzed in terms of plausible spatial distribution models that aim to separate the disk component from the Galactic Bulge component [see Fig 2.14 (Purcell et al., 1997; Milne et al., 2000)]. This decomposition implies annihilation rates of 10^{43} e^+ s^{-1} for the disk and 2.6×10^{43} e^+ s^{-1} for the bulge. Almost all of the annihilation luminosity from the Galactic Disk may be explained by radioactive sources. About $16 \pm 5\%$ is assigned to ^{26}Al, with the remainder partitioned between ^{44}Ti, ^{56}Co, and old stellar population products. The estimated positronium fraction of 0.94–1.0 for the inner Galaxy suggests that the contribution from compact sources might be small. However, this constraint strongly depends on the environment of the compact sources: for example, the entire bulge component could be explained from jet sources exemplified by the 'Great Annihilator'[18] alone if positrons are not rapidly annihilated in a target close to that compact source (Ramaty et al., 1994). Estimates of the contribution from compact sources may also be derived from simulations of classical novae. These show that the peak 511 keV emission reaches $\sim10^{-2}$ (D/1 kpc)^2 photons cm^{-2} s^{-1} for a period of about 7 h after the outburst (Gomez-Gomar et al., 1998). This would make nova detections from distances as far as the Galactic Center feasible, if the timing of the observations were fortunate. Overall, however, the nova contribution to the diffuse 511 keV glow of the Galaxy is expected to be low.

[18] This source 1E1740.7-2942 had been understood to inject a large number of positrons through its jets, which have been mapped by radio observations. The large amount of experimental data on the inner-Galaxy 511 keV intensity had suggested time variability on the scale of a few months. Later these measurements were explained consistent with time invariable flux; differing instrumental fields of view and backgrounds explain the different measured flux values.

Spectral decomposition of the γ-ray spectrum from the inner Galaxy is difficult, in particular for extraction of the three-photon continuum from positronium annihilation (Kinzer et al., 1999), which is crucial for extraction of a radioactivity- or nucleosynthesis-related signal. Problems arise from the diffuse Galactic continuum emission (see Chap 9), beyond the uncertain contribution from variable hard X-ray sources such as seen by the French SIGMA coded-mask X-ray telescope aboard the Russian GRANAT satellite. Therefore the uncertainty from spectral analysis alone remains large, and imaging results are needed.

The OSSE team reported a spectacular result from their efforts to map the annihilation emission of the inner Galaxy, using their many pointings during the CGRO mission (Purcell et al., 1997). According to their interpretation, a 'fountain' of positrons appears to emerge from the inner Galaxy and annihilate over a region extending several 100 pc into the northern halo. Imaging analysis is very difficult for such data from a nonimaging collimator instrument, and some care should be applied in interpretations. Nevertheless, this inner region of the Galaxy appears to have interesting peculiarities, also from other observational hints such as EGRET and SIGMA results (see also Chaps 4 and 13), and models for a positron jet source have been advocated (Dermer and Skibo, 1997). Better imaging measurements of annihilation γ-rays are needed.

10.5 Summary and Perspective

Nucleosynthesis bridges many aspects of modern astrophysics, from the basic nuclear physics processes and studies of stars and supernovae to investigations of chemical evolution throughout galaxies and the universe. Gamma-ray observations have joined this field, with a significant boost from the CGRO, through discoveries of several γ-ray lines with measurements of spatial distributions and line shapes. Although the astronomical precision of these measurements lags far behind what has been achieved in other fields, the more direct constraints set by γ-ray lines have distinct advantages over other approaches to understand the sites of nucleosynthesis in the different places in the evolving universe.

We have seen that supernova light is powered by radioactivity at very different time scales, from early ^{56}Ni to late ^{44}Ti and positrons. The puzzling observation of ^{44}Ti from exceptional supernovae may turn out to give fundamentally new insight on processes close to the compact remnant of a core collapse. We learn that massive stars can be probed through ^{26}Al decay γ-rays throughout otherwise opaque regions. We have obtained a glimpse of the potential information carried by different line shapes of the radioactivity γ-rays. The γ-ray universe has shown once more that 'color' information educates us about the variety and detail of fundamental physical processes, in the regime of γ-rays, as in other domains of the electromagnetic spectrum.

What remains is reconciliation of these lessons with our models of the sites of nucleosynthesis, such that we can sufficiently refine those models to explain isotopic abundances as they evolved from the Big Bang to sites we observe today.

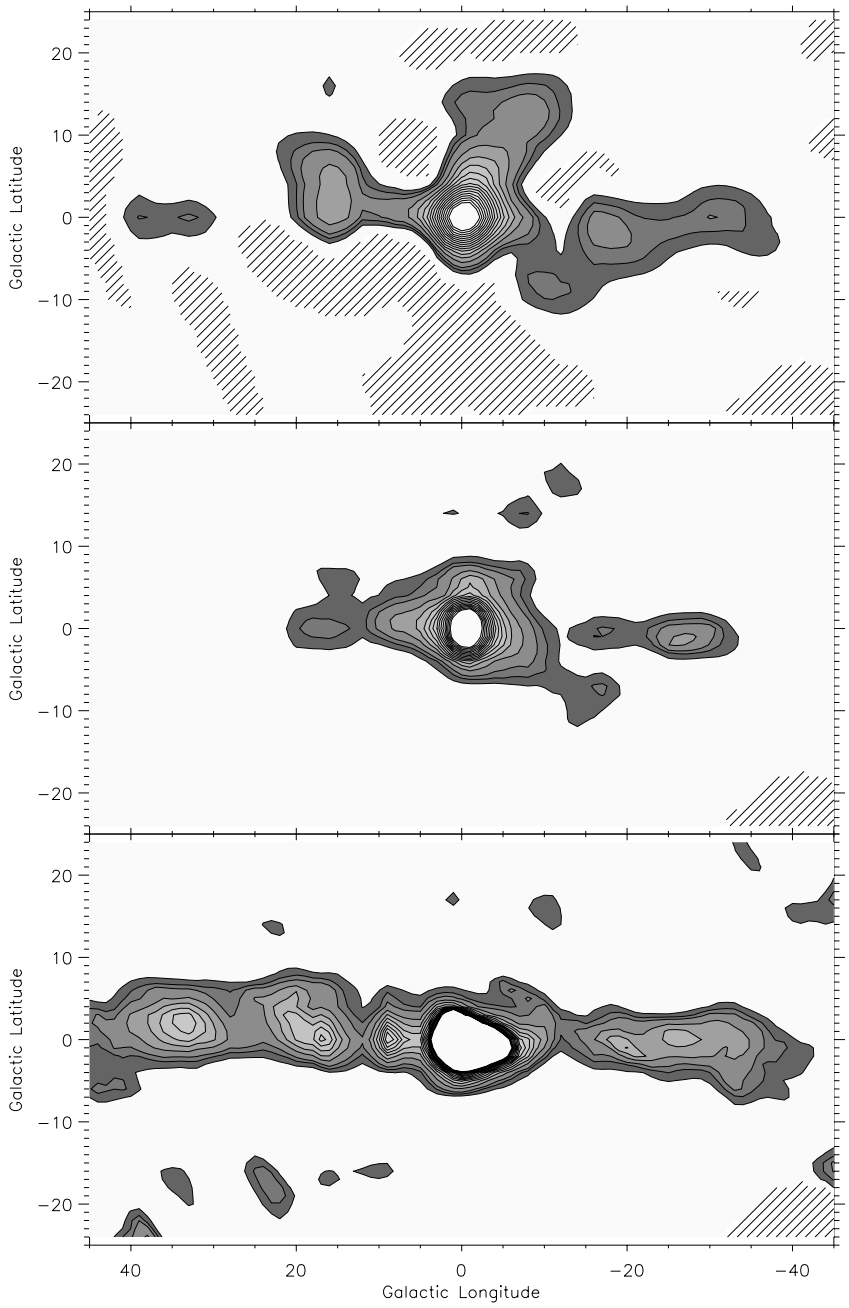

Fig. 10.14. Annihilation radiation images from the inner Galaxy region (Milne et al., 2000). The two upper maps show 511 keV line data from the nonimaging instruments OSSE and SMM, deconvolved into an intensity map with two different techniques. The lower panel shows the continuum annihilation emission measured with OSSE below the 511 keV line, and demonstrates that here the disk of the Galaxy has a larger contribution. Reproduced with permission from Milne et al. 2000

Bibliography

Anders E., Grevesse , 1989, Geochim. Cosmochim. Acta, 53, 197

Arnett W.D., 1996, *Supernovae and Nucleosynthesis*, Princeton: Princeton University Press

Arnett W. D. et al., 1977, Ann.NY Acad.Sci., 302, 90

Arnould M., Takahashi K., 1999, Rep. Prog. Phys., 62, 395

Aschenbach B., 1998, Nature, 396, 141

Aschenbach B., Iyudin A.F., Schönfelder V., 1999, Astron. Astrophys. 350, 997

Bernatowicz T.J., Walker R.M., 1997, Phys.Today, 12, 26

Branch D., 1998, Annu. Rev. Astron. Astrophys. 36, 17

Burbidge E. M., Burbidge G. R., Fowler W. A., and Hoyle F., 1957, Rev. Mod. Phys. 29, 547

Burrows A., 2000, Nature 403, 727

Bussard R.W., Ramaty R., Brachman R.J., 1979, Astrophys. J. 228, 928

Cameron A. G. W., 1957, Chalk River Report, CRL-41

Chan, K. and Lingenfelter, R., 1991, Astrophys. J., 368, 515

Chan K., and Lingenfelter, R., 1993, Astrophys. J., 405, 614

Clayton D. D., 1968, *Principles of Stellar Evolution and Nucleosynthesis*, New York: Mac Graw-Hill

Clayton D. D., Colgate S. A., and Fishman G., 1969, Astrophys. J., 220, 353

Del Rio E., von Ballmoos P., Bennett K., et al., 1996, Astron. Astrophys., 315 237

Dermer C.D., Skibo J.G., 1997, Astrophys. J. 487, L57

Diehl R., Dupraz C., Bennett K., et al., 1995, Astron. Astrophys. 298, 445

Diehl R., Wessolowski U., Oberlack U., et al. 1997, AIP Conf. Proc. 410, 1109

Diehl R., and Timmes F.X., 1998, Publ. Astron. Soc. Pac. 110, 748, 637

Diehl R., Oberlack U., Plüschke S., et al. 1999, Astroph. Letters and Communications, 38, 357

Dupraz C., Bloemen H., Bennett K., et al., 1997, Astron. Astrophys. 324, 683

Forestini M., and Charbonnel C., 1997, Astron. Astrophys.S, 123, 241

Gamow G.Z., 1928, Z. Phys. 51, 204

Gehrels N., Leventhal M., MacCallum C.J., 1988, AIP Conf. Proc. 170, 87

Gehrz R., Truran J., Williams R., Starrfield S., 1998, Publ. Astron. Soc. Pac. 110, 3

Gomez-Gomar J., Hernanz M., Jose J., Isern J., 1998, Mon. Not. R. Astron. Soc. 296, 913

Georgii R., Plüschke S., Diehl R., et al., 2000, AIP Conf. Proc. 510, 49

Harris M.J., Leising M.D., Share G., 1991, Astrophys. J. 375, 216

Hartmann D. H., Predehl P., Greiner J., et al., 1997, Nucl. Phys. A 621, 83

Hernanz M., Gomez-Gomar J., José J., Isern J., 1997, ESA-SP 382, 47

Hix W.R., and Thielemann F.-K., 1999, Astrophys. J. 511, 862
Iben I., and Renzini A., 1983, Annu. Rev. Astron. Astrophys. 21, 271
Iwamoto K., Brachwitz F., Nomoto K., Kishimoto N., 1999, Astrophys. J.S 125, 439
Iyudin A. F., Diehl R., Bloemen H., et al., 1994, Astron. Astrophys. 284, L1
Iyudin A. F., Bennett K., Bloemen H., et al., 1995, Astron. Astrophys. 300, 422
Iyudin A., Schönfelder V., Bennett K., et al., 1998, Nature 396, 142
José J., Hernanz M., 1997, Nucl. Phys. A 621, 491
Käppeler F., Beer H., and Wishak K., 1989, Rep. Prog. Phys. 52, 945
Kinzer R.L., Purcell W.R., Kurfess J.D., 1999, Astrophys. J. 515, 215
Kirsten T., 1999, Rev. Mod. Phys. 71, 1213
Knödlseder J., 1999, Astrophys. J., 510, 915
Knödlseder J., Dixon D.D., Diehl R., et al., 1999a, Astron. Astrophys. 345, 813
Knödlseder J., Bennett K., Bloemen H., et al., 1999b, Astron. Astrophys. 344, 68
Kolb U., and Politano M., 1997, Astron. Astrophys. 319, 909
Kurfess J. D., Johnson W. N., Kinzer R. L., et al., 1992, Astrophys. J. 399, L137
Lattanzio J.C., and Boothroyd A.I., 1997, AIP Conf. Proc. 402, 85
Leising M. D., and Share G. H., 1994, Astrophys. J. 424, 200
MacPherson G. J., Davis A. M., and Zinner E. K., 1995, Meteoritics 30, 365
Merill P.W., 1952, Science 115, 484
Meyer B.S., 1993, Phys. Rep. 227, 1-5, 257
Meyer B.S., 1994, Annu. Rev. Astron. Astrophys. 32, 153
Meynet G., Arnould M., Prantzos N., Paulus G., 1997, Astron. Astrophys. 320, 460
Milne P., et al., 2000, AIP Conf. Proc. 510, 21
Mochizuki Y., Takahashi K., Janka H.-Th., et al., 1999, Astron. Astrophys. 346, 831
Morris D. J., Bennett K., Bloemen H., et al., 1995, 17th Texas Symposium, N.Y. Acad. Sci., 759, 397
Naya J.E., Barthelmy S.D., Bartlett L.M., et al., 1996, Nature 384, 44
Naya J.E., Barthelmy S.D., Bartlett L.M., et al., 1998, Astrophys. J. 499, L169
Niemeyer J., 1999, Astrophys. J. 523, 57
Nomoto K., Iwamoto K., Kishimoto N., 1997, Science 276, 1378
Oberlack U., Wessolowski U., Diehl R., et al., 1999, Astron. Astrophys. 353, 715
Pagel B.E.J., 1997, *Nucleosynthesis and Chemical Evolution in Galaxies*, Cambridge: Cambridge University Press
Prantzos N., Diehl R., 1996, Phys. Rep. 267, 1
Purcell W. R., Cheng L.-X., Dixon D. D., et al., 1997, Astrophys. J. 491, 725
SN 1987A: Ten Years After, The Fifth CTIO/ESO/LCO Workshop, 2000, eds M. M. Phillips & N. B. Suntzeff,ASP, in preparation
Qian Y-Z., Woosley S.E., 1996, Astrophys. J. 471, 331
Ramaty R., Skibo J.G., and Lingenfelter R.E., 1994, Astrophys. J.S 92, 393
Ramaty R. and Lingenfelter R. E., 1977, Astrophys. J. 213, L5
Ramaty R., Kozlovsy B., and Lingenfelter R.E., 1999, Phys. Today 4, 30
Ritossa C., Garcia-Berro E., Iben I., 1996, Astrophys. J. 460, 489
Rohlfs C., and Rodney W. 1988, *Cauldrons in the Cosmos*, Chicago: Univ. of Chicago Press
Schatz H., Aprahamian A., Görres J., et al., 1998, Phys. Rep. 294 (4), 198
Schramm D.N., Turner M.S., 1998, Rev. Mod. Phys. 70, 1, 303
Shu F.H., Adams F.C., Lizano F., 1987, Annu. Rev. Astron. Astrophys. 25, 84

Simpson J.A., Connell J.J., 1998, Astrophys. J. 497, L85
Suess H.E.P., and Urey H.C., 1956, Rev. Mod. Physics 28, 53
Stone E. C., Cohen C. M. S., Cook W. R., et al., 1998, Sp. Sci. Rev. 86, 357
The L.-S., Diehl R., Hartmann D.H., et al., 2000, AIP Conf. Proc. 510, 64
Thielemann F. -K., Nomoto K., and Yokoi Y., 1986, Astron. Astrophys. 158, 17
Thielemann F. -K., Nomoto K., and Hashimoto M. A., 1996, Astrophys. J. 460, 408
Timmes F. X., Woosley S. E., Hartmann D. H., et al., 1995, Astrophys. J. 449, 204
Timmes F. X., Woosley S. E., Hoffman R. D., Hartmann D. H., 1996, Astrophys. J. 464, 332
Trimble V., 1975, Rev. Mod. Phys. 47, 877
Trimble V., 1991, Astron. Astrophys. Rev. 3, 1
Tutukov A. V., Yungelson L. R., and Iben I. Jr., 1992, Astrophys. J. 386, 197
Wallerstein G., Iben I., Parker P., et al., 1997, Rev. Mod. Phys. 69, 4, 995
Woosley S. E., Hartmann D. H., Hoffman R. D., and Haxton W. C. 1990, Astrophys. J. 356, 272
Woosley S. E., and Weaver T. A., 1995, Astrophys. J.S 101, 181
Woosley S.E., 1997, Astrophys. J. 476, 801